

Harnessing optical forces with advanced nanophotonic structures: principles and applications

Geze Gao¹ · Tianhua Shao¹ · Tianyue Li¹ · Shuming Wang¹

Received: 26 January 2025 / Accepted: 9 April 2025

Published online: 03 May 2025

© The Author(s) 2025 OPEN

Abstract

Non-contact mechanical control of light has given rise to optical manipulation, facilitating diverse light-matter interactions and enabling pioneering applications like optical tweezers. However, the practical adoption of versatile optical tweezing systems remains constrained by the complexity and bulkiness of their optical setups, underscoring the urgent requirement for advancements in miniaturization and functional integration. In this paper, we present innovations in optical manipulation within the nanophotonic domain, including fiber-based and metamaterial tweezers, as well as their emerging applications in manipulating cells and artificial micro-nano robots. Furthermore, we explore interdisciplinary on-chip devices that integrate photonic crystals and optofluidics. By merging optical manipulation with the dynamism of nanophotonics and metamaterials, this work seeks to chart a transformative pathway for the future of optomechanics and beyond.

Keywords Optical manipulation · Fiber optical tweezers · Plasmonic tweezers · Metasurface tweezers · Metamotors · Biological manipulation

1 Introduction

Beyond merely conveying information from the external world, light also transfers energy and momentum when interacting with matter. This transfer of linear and angular momentum of light to matter results in optomechanical effects known as optical forces, which can be exerted on particles, cells, and even single molecules, enabling non-contact trapping, transport, sorting, and analysis at the microscale, and accordingly, it has given rise to the field of optical manipulation. Optical tweezers (OT), the famous invention for optical manipulation, was firstly proposed by Arthur Ashkin in the early 1970s [1]. Conventional OT rely on the gradient force generated by a tightly focused laser beam to trap particles near the focal point [2]. The ability to apply piconewton-level forces and measure nanometer-level displacements has made OT a powerful technique for studying biological systems at the single-molecule level. For example, OT have been used to measure the mechanical properties of DNA [3], study the force generation and stepping behavior of molecular motors such as kinesin [4] and myosin [5], and probe the viscoelastic properties of cells [6]. OT have also found applications in physics and materials science, such as investigating colloidal interactions [7], manipulating nanostructures [8], and even cooling atoms to ultra-low temperatures [9].

Geze Gao and Tianhua Shao have contributed equally to this work.

✉ Tianyue Li, leos4a@163.com; ✉ Shuming Wang, wangshuming@nju.edu.cn | ¹National Laboratory of Solid-State Microstructures, Collaborative Innovation Center of Advanced Microstructures, School of Physics, Nanjing University, Nanjing 210093, China.



Despite their wide-ranging applications, conventional OT operating in free space have some limitations. The bulky and complex setup, involving high-numerical-aperture (NA) objective lenses and precise alignment, can hinder their integration with other techniques and limit their use in certain environments. To overcome these, fiber-based OT have emerged as a more flexible and miniaturized alternative. By integrating optical trapping with fiber optics, it is possible to create compact and portable devices that can be easily incorporated into microfluidic systems, endoscopes [10], and even implanted in living organisms [11]. Fiber-based OT have been used for various applications, including cell manipulation [12], particle sorting [13], and *in vivo* trapping [14].

In addition to fiber-based OT, novel optical manipulation techniques have been developed based on engineered optical fields and microstructures, such as subwavelength metamaterials (MM) and Metasurfaces (MS) [15–30], enabling unusual light fields to provide optical forces, including pulling forces [31], lateral forces [32] and so on [33]. By carefully designing the geometry and arrangement of MM structures, it is possible to generate complex optical force landscapes that can trap, sort, and manipulate particles in ways not achievable with conventional OT. Plasmonic nanostructures have also been exploited for optical trapping, leveraging the strong field enhancements and localized hotspots generated by surface plasmons [34].

Optical manipulation has found extensive applications in biology and medicine, particularly in the area of cell mechanics and mechanobiology. The ability to apply precise forces to individual cells and measure their mechanical responses has provided valuable insights into the role of mechanical cues in cell function and disease [35]. OT have been used to study the mechanical properties of various cell types, including red blood cells, cancer cells, and stem cells. By combining optical trapping with microfluidic devices (MFD), high-throughput cell sorting and analysis based on mechanical properties have been demonstrated. This has potential applications in disease diagnosis, drug screening, and regenerative medicine. The use of optical forces to drive and control micromachines and microrobots is another exciting area of optical manipulation. By designing microstructures that can efficiently convert light into mechanical motion, researchers have developed various types of light-driven micromotors [36], microswimmers [37], and microactuators [38]. These microrobots can be remotely controlled using structured light fields and can perform complex tasks such as cargo transport [39], cell manipulation and targeted drug delivery [40]. The combination of optical micromanipulation with smart materials and stimuli-responsive polymers has further expanded the capabilities of these microrobotic systems [41].

The field of optofluidics (OF), which synergistically combines optics and fluidics, has greatly benefited from advances in optical micromanipulation [42]. By integrating optical trapping and manipulation capabilities into MFD, it is possible to perform particle sorting [43], analysis [44], and assembly [45] on a chip. OF devices have been used for various applications, such as cell cytometry [46], biosensing [47], and droplet manipulation [48]. The integration of optical waveguides (WG), photonic crystals (PhC), and PN structures into OF devices has enabled novel functionalities and enhanced performance [49].

Photonic integrated circuits (PICs) offer a promising platform for scalable and efficient optical manipulation [50]. By miniaturizing and integrating optical components on a chip, PICs can generate complex optical fields and force landscapes for particle trapping and manipulation [34]. PICs have been used to create arrays of optical traps [51], sort particles based on their optical properties [52], and even perform quantum operations on trapped atoms [53]. The integration of PICs with MFD and electronic control circuitry can enable programmable and reconfigurable optical manipulation systems with applications in lab-on-a-chip devices and high-throughput screening [54].

2 Optical forces arising from nanophotonic devices

2.1 Waveguide theory in optical fibers

Optical fibers generally consist of a core that guides light, a cladding that provides total internal reflection conditions within the core, and a coating that protects the bare fiber from external micro-strain and waterproofing. Optical fibers can be divided into ultraviolet optical fibers, visible optical fibers and infrared optical fibers according to their working wavelengths; According to the refractive index distribution, it can be divided into step index fiber (SIF) and gradient index fiber (GIF) the refractive index of the core of the SIF and the refractive index of the cladding are constants, and the refractive index of the fiber core to the cladding is abrupt. For stepped multimode fibers, the transmission paths of the various modes are different, and the time to reach the end point after transmission is also different, resulting in a delay difference and a pulse broadening. Therefore, the inter-mode dispersion of this optical fiber is high, the transmission frequency band is not wide, and the transmission efficiency is not high. The refractive

index of the core of the graded optical fiber decreases regularly with the increase of the radius, and decreases to the refractive index of the cladding at the junction of the core and the cladding, and the refractive index change of the core is similar to that of a parabola:

$$n_{(r)} = \begin{cases} n_1 \sqrt{1 - 2\Delta \left(\frac{r}{a}\right)^g} & (r < a) \\ n_2 & (r \geq a) \end{cases} \quad (1)$$

According to the number of transmission modes, it can be divided into single-mode fiber (SMF), few-mode fiber (FMF) and multi-mode fiber (MMF). The number of modes allowed in a fiber can be estimated based on the following formula:

$$M = \frac{g}{2g+2} V^2 \quad (2)$$

where V is the normalized frequency of the fiber and g is the refractive index distribution parameter. In a step fiber, if $V < 2.405$, it can only accommodate a single mode, known as the main mode or base mode. Single-mode optical fiber can only transmit fundamental mode, without inter-mode dispersion, suitable for long-distance communication, but single-mode optical fiber has high requirements for the spectral width and stability of the light source. Multimode optical fibers can transmit multiple modes of light, and the inter-mode dispersion is large, which limits the frequency of transmitting digital signals, and the loss increases with the increase of distance. According to the polarization state of transmission, single-mode optical fiber can be divided into polarization-maintaining fiber and non-polarization-maintaining fiber, and the difference between the two lies in whether polarized light can be transmitted.

The refractive index distribution of the cross-section of the optical fiber is generally circularly symmetrical, and the light guiding principle of the optical fiber can be analyzed by wave theory. Let the guided wave propagate in the $+z$ direction, E_z and H_z satisfy the scalar Helmholtz equation:

$$\begin{cases} \nabla^2 E_z + k_0^2 n^2 E_z = 0 \\ \nabla^2 H_z + k_0^2 n^2 H_z = 0 \end{cases} \quad (3)$$

The refractive indices in the core and cladding are n_1 ($r < a$) and n_2 ($r \geq a$), respectively. where $k = \omega \sqrt{\mu \epsilon} = \omega \sqrt{\mu_0 \mu_r \epsilon_0 \epsilon_r} = k_0 n$, $k_0 = \omega \sqrt{\mu_0 \epsilon_0} = \frac{2\pi}{\lambda_0}$, E_z in Eq. (3) is obtained by expanding it in the column coordinate system and separating the variables:

$$E_z(r, \theta, z) = AR(r)\Theta(\theta)Z(z) \quad (4)$$

$Z(z)$ represents the axial variation of the guided wave along the fiber, β represents its axial phase constant, $\Theta(\theta)$ is the variation law of E_z along the circumferential direction, and the variation law of the guided wave along the circumferential direction, according to the symmetry of the natural have:

$$Z(z) = -Ae^{i\beta z} \quad (5)$$

$$\Theta(\theta) = \begin{cases} \cos m\theta \\ \sin m\theta \end{cases} \quad (6)$$

$R(r)$ is the change in the radial direction of the guided wave:

$$r^2 \frac{d^2 R(r)}{dr^2} + r \frac{dR(r)}{dr} + [(k_0^2 n^2 - \beta^2)r^2 - m^2]R(r) = 0 \quad (7)$$

In the core, it should be an oscillatory solution, so the Bessel function is taken; In the cladding, it is a decay solution, so the second type of modified Bessel function solution is taken.

$$R(r) = \begin{cases} J_m\left(\sqrt{n_1^2 k_0^2 - \beta^2} r\right) & (r \leq a) \\ K_m\left(\sqrt{\beta^2 - n_2^2 k_0^2} r\right) & (r \geq a) \end{cases} \quad (8)$$

J_m is the m-order Bessel function, and K_m is the second-class m-order Bessel function. U is the radially normalized phase constant of the guided wave, which describes the distribution of the electric and magnetic fields of the guided wave across the cross-section of the core. W is the radially normalized attenuation constant of the guided wave, which describes the distribution of the electric and magnetic fields of the guided wave over the cross-section of the cladding. β is the phase constant of the guided wave as it travels along the optical fiber axial.

$$\begin{cases} U = \sqrt{n_1^2 k_0^2 - \beta^2} a & (r \leq a) \\ W = \sqrt{\beta^2 - n_2^2 k_0^2} a & (r \geq a) \end{cases} \quad (9)$$

Let the frequency of the fiber be normalized: $V = \sqrt{U^2 + W^2} = \sqrt{n_1^2 - n_2^2} k_0 a = \sqrt{2\Delta} n_1 k_0 a = \frac{2\pi}{\lambda_0} \sqrt{2\Delta} n_1 a$. W is a parameter representing how fast or slow the guided wave decays radially in the cladding. When $W \rightarrow 0$, the guided wave field does not decay in the cladding, and the guided wave is converted into a radiant wave, that is, the guided wave is cut off. When $W \rightarrow \infty$, the guided wave field attenuates the most in the cladding, and the optical fiber has the strongest ability to restrain the guided wave, that is, the guided wave is far away from the cutoff. V is a physical quantity that reflects the magnitude of the optical frequency without dimension, which is related to the structural parameters and working wavelength of the optical fiber, the larger the V value, the more the number of guided waves, the easier it is to meet the transmission conditions, and it is far away from the cut-off. If $V \rightarrow \infty$, the guided wave field is completely concentrated in the core and the field in the cladding is zero. As the V value decreases, the light field will stretch into the cladding, and some modes will gradually leak to the outer surface of the fiber and be lost, which is called pattern cutoff.

By substituting the expressions of $R(r)$, $\Theta(\theta)$ and $Z(z)$ into Eq. (4) and the relationship between U and W , using the boundary conditions of the fiber: $E_{z1} = E_{z2}$ and $H_{z1} = H_{z2}$ at $r = a$. The distribution function of E_z versus Hz can be obtained:

$$\begin{cases} E_{z1}(r, \theta, z) = A e^{-j\beta z} \sin m\theta \frac{J_m\left(\frac{Ur}{a}\right)}{J_m(U)} & (r \leq a) \\ H_{z1}(r, \theta, z) = B e^{-j\beta z} \cos m\theta \frac{J_m\left(\frac{Ur}{a}\right)}{J_m(U)} & (r \leq a) \\ E_{z2}(r, \theta, z) = A e^{-j\beta z} \sin m\theta \frac{K_m\left(\frac{Wr}{a}\right)}{K_m(W)} & (r \geq a) \\ H_{z2}(r, \theta, z) = B e^{-j\beta z} \cos m\theta \frac{K_m\left(\frac{Wr}{a}\right)}{K_m(W)} & (r \geq a) \end{cases} \quad (10)$$

At the interface between the core and the cladding, the tangential direction of the electric field and the magnetic field is continuous, and the guided wave equation in the fiber can be obtained:

$$\left[\frac{n_1^2}{n_2^2} \frac{1}{U} \frac{J'_m(U)}{J_m(U)} + \frac{1}{W} \frac{K'_m(W)}{K_m(W)} \right] \times \left[\frac{1}{U} \frac{J'_m(U)}{J_m(U)} + \frac{1}{W} \frac{K'_m(W)}{K_m(W)} \right] = m^2 \left(\frac{1}{U^2} + \frac{1}{W^2} \right) \left(\frac{n_1^2}{n_2^2} \frac{1}{U^2} + \frac{1}{W^2} \right) \quad (11)$$

For weakly conductive fibers which $n_2 \approx n_1$, the characteristic equation can be simplified as:

$$\frac{1}{U} \frac{J'_m(U)}{J_m(U)} + \frac{1}{W} \frac{K'_m(W)}{K_m(W)} = \pm m \left(\frac{1}{U^2} + \frac{1}{W^2} \right) \quad (12)$$

The characteristic equations of the four modes of TE, TM, HE, and EH in the optical fiber can be obtained by using the characteristic equations:

TE:

$$\frac{1}{U} \frac{J'_0(U)}{J_0(U)} + \frac{1}{W} \frac{K'_0(W)}{K_0(W)} = 0 \quad (13)$$

TM:

$$\frac{n_1^2}{U} \frac{J'_0(U)}{J_0(U)} + \frac{n_2^2}{W} \frac{K'_0(W)}{K_0(W)} = 0 \quad (14)$$

HE_{mn}:

$$\frac{1}{U} \frac{J_{m-1}(U)}{J_m(U)} = \frac{1}{W} \frac{K_{m-1}(W)}{K_m(W)} \quad (15)$$

EH_{mn}:

$$\frac{1}{U} \frac{J_{m+1}(U)}{J_m(U)} = -\frac{1}{W} \frac{K_{m+1}(W)}{K_m(W)} \quad (16)$$

Through the characteristic equation, a series of U or W , β values that satisfy the equation can be obtained, and various modes that can be transmitted in the optical fiber can be obtained, and then the normalized cut-off frequency V_c and transmission characteristics of various modes can be obtained.

2.2 Fiber optical tweezers

When a high-intensity laser beam irradiates dielectric particles, the momentum generated by the scattering of incident photons produces an optical force on the particles near the focus, which can be divided into scattering force and gradient force. The gradient optical field formed by the converging laser can cause refraction, reflection, absorption, and other effects in objects, forming an optical potential well to capture objects near the focal point of the optical field. Optical tweezers have the characteristics of non-invasiveness, non-destructiveness, and ultra-high sensitivity. Since Ashkin et al. designed the traditional optical tweezers in 1969 [1], which achieved stable capture of particles using two counter-propagating focused beams, optical tweezers systems have been continuously upgraded over the past 60 years. The core approach to enhance the capture ability is to improve the focusing capability of the laser by designing the optical path or optical elements or to enhance the gradient optical field by designing certain structures. Optical fiber tweezers use optical fibers to replace part of the optical path in traditional optical tweezers based on high-resolution microscope objectives. Due to the more convenient operation of optical fiber probes, it greatly reduces the operational difficulty caused by adjusting various optical devices and lenses in traditional optical tweezers. Moreover, optical fiber tweezers have a small volume and are easy to integrate into microfluidic channels or photonic chips. Up to now, according to the operation methods and principles, optical fiber tweezers can be roughly divided into dual-fiber optical tweezers, single-fiber optical tweezers, and optical fiber tweezers based on special fiber cores.

2.2.1 Dual-fiber optical tweezers

In 1993, A. Constable et al. first used two diode lasers with optical fibers to achieve a dual-fiber optical tweezers device with functions similar to traditional optical tweezers based on high-resolution microscope objectives. They captured polystyrene microspheres with diameters of 0.1–10 μm by the synergistic scattering forces of two beams propagating in opposite directions [55]. Since light passing through ordinary single-mode fibers and entering free space leads to beam divergence, in 1995, Lyons et al. designed the tips of two optical fibers into a conical shape, which is more conducive to light focusing and forms a larger gradient force at the focal point [56]. The advantages of dual-fiber optical tweezers lie not only in the larger capture force and wider capture range at the focal point but also in the adaptability of the optical fiber probes to high refractive index environments [57]. By utilizing the stable equilibrium point formed below the intersection of the beams from two fibers, the movement range of the captured object can be effectively controlled, and the risk of mechanical damage to the captured object due to contact with the fiber probe can be avoided. In addition to

the capture function, dual-fiber optical tweezers can also serve as optical fiber stretchers, i.e., by placing the object at the optical force equilibrium point and changing the magnitude of the equilibrium force to alter the surface tension of the captured object, thereby changing its shape. This allows non-invasive measurement of the Young's modulus of cells and organelles, enabling cell classification based on cytoskeleton characteristics. For example, cancer cells are more easily deformed than healthy cells, so cancer diagnosis can be achieved by measuring the optical deformability of cells. Since optical stretchers are generally used for living cell measurements, the optical power used for optical stretchers needs to be controlled within a certain range to avoid causing greater damage to cells and organelles [58, 59]. In addition to manipulating particles in liquid environments, dual-fiber optical tweezers can also manipulate aerosols in air [60], which can be applied to fields such as atmospheric chemistry.

Apart from the above functions, the applications of dual-fiber optical tweezers also include manipulating object assembly [61], sensing and tracking object positions [62, 63], optical fiber wrenches [64], etc. When dual-fiber optical tweezers are used to manipulate object assembly, multiple particles are captured simultaneously, and each particle affects the optical field distribution of other particles [61]. Therefore, these particles rearrange to reach a stable state with the lowest system energy. The arrangement of particles strongly depends on their size. Larger particles tend to squeeze each other along the axis, while smaller particles tend to form evenly spaced chain structures. The sensing of target object positions by dual-fiber optical tweezers is mainly based on the intensity variation of the scattering force generated by the optical fiber trap [62]. Two beams form a stable trap that fixes the object at a specific position. When the object moves, the intensity of the scattered and transmitted light from the fiber changes. By collecting the spectral data of the scattered and transmitted light with a spectrometer, the position of the object can be determined. For cells undergoing random Brownian motion due to thermal motion, a pair of orthogonal quadrant photodiodes can also be used to detect the laser scattered by the cells and convert it into an electrical signal [63]. By analyzing the Brownian motion of the cells, the force constants of the optical force field can be determined. These force constants describe the magnitude of the restoring force experienced by the cells in each direction in the optical trap. By calculating these force constants, the stability of the cells in the optical tweezers and the strength of the optical force field can be understood (Fig. 1).

Optical fiber wrenches apply torque to objects by controlling the relative position and intensity of two counter-propagating lasers, one of which is emitted through a dual-mode fiber. By fusing a single-mode fiber and a dual-mode fiber with a certain offset, an asymmetric laser beam is generated [64]. When this asymmetric laser beam rotates, the asymmetry causes the captured cell to rotate along the intensity gradient of the beam, thereby driving the captured particle to rotate around an optical axis perpendicular to the microscope. The rotation angle can range from 5 to 180°. In medicine, this non-contact function of controlling cell rotation can be used to achieve single-cell tomography. In recent

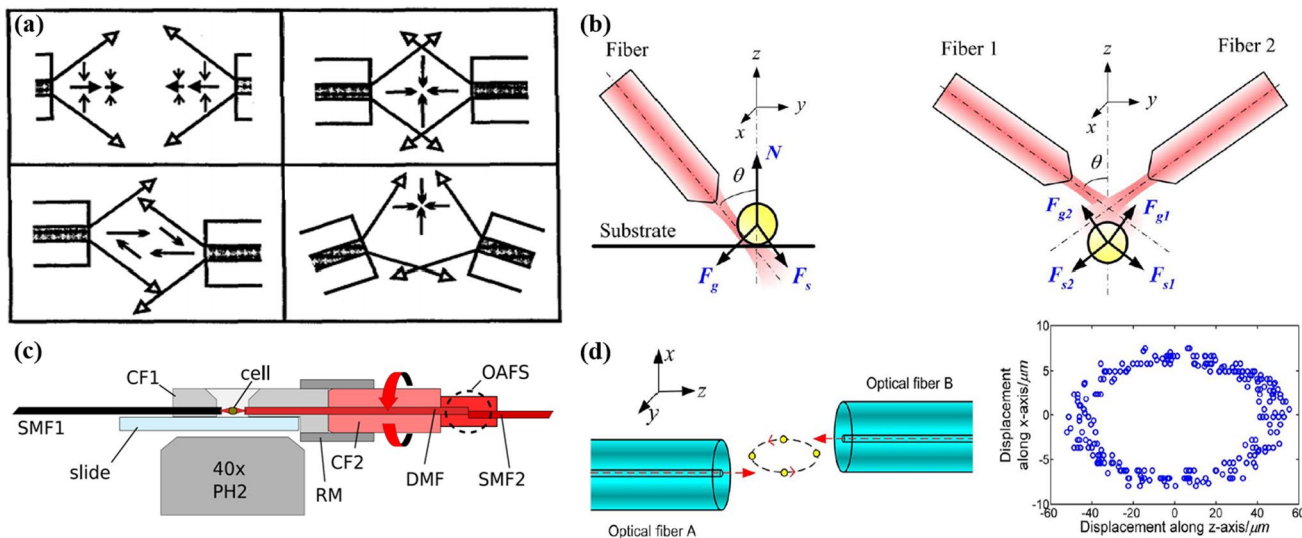


Fig. 1 **a** The direction of the gradient and scattering forces in the optical force trap, and the direction of the total force when the fiber alignment is not perfect [55]. **b** Schematic diagram of cone-tip single-fiber optical tweezers and dual-fiber optical tweezers applying force to trapped particles [65]. **c** Schematic diagram of optical cell rotator (OCR) setup [64]. **d** A double fiber optical tweezers for optical orbit rotation in a transversally misaligned double fiber optical trap, and a two-dimensional projection of the trajectory of the captured particle in the x-z plane [66]

years, researchers have been continuously improving the capabilities of dual-fiber optical tweezers, such as by tilting dual-fiber optical tweezers [65], laterally misaligning dual-fiber optical tweezers [66], and using 3D-printed diffractive Fresnel lenses on the fiber end face to generate converging beams [67]. These improvements make dual-fiber optical tweezers less complex and difficult to manipulate in three-dimensional space and enable the capture and manipulation of particles over a wider size range. In addition, Jiang et al. [68] studied the influence of different fiber modes and conical fiber angles on the capture force of dual-fiber optical tweezers, proving that the optical capture force of the fundamental mode is greater than that of higher-order modes. They obtained the optimal angle that maximizes the optical capture force by optimizing the conical fiber angle.

In summary, dual-fiber optical tweezers technology shows potential in capturing and manipulating multiple particles. In the future, more complex multi-particle manipulation and self-assembly functions can be explored. Moreover, dual-fiber optical tweezers have broad application prospects in the capture and analysis of biological samples, such as in cell biology, drug delivery, and biomechanics research.

2.2.2 Single-fiber optical tweezers

Dual-fiber optical tweezers require synchronous and precise adjustment of two fibers during operation, utilizing counter-propagating scattering forces to manipulate particles. However, the gradient force generated by a single fiber can also achieve similar manipulation functions as dual-fiber optical tweezers. In 1997, Taguchi et al. first used a single fiber to manipulate microparticles [69]. In single-fiber optical tweezers, a highly focused laser beam is transmitted through the fiber to the tip of the probe, forming a strong optical field at the tip. When the beam illuminates the particle, the light is scattered by the particle, and the scattering force F_s pushes the particle away from the focus, transferring momentum from the photons to the particle. The gradient force F_g is caused by the spatial variation of the beam intensity. When the particle is in a region with a high optical intensity gradient, it experiences a force pushing it towards the beam focus, i.e., the region with the highest optical intensity, as shown by Fig. 2a. To achieve stable capture, the scattering force and gradient force need to be balanced. When the particle deviates from the optical axis, the gradient force pulls it back to the beam center, while the scattering force helps the particle maintain its position along the propagation direction of the beam. By adjusting the power of the laser source and the position of the fiber, the position and motion of the particle can be precisely controlled, thereby manipulating the particle [70], as shown by Fig. 2b, c. In 2006, Eom et al. achieved three-dimensional probing using single-fiber optical tweezers [71], using a fiber and a microsphere to replace the traditional probe, with the fiber as the probe rod and the microsphere as the probe ball. The microsphere is captured by the optical force at the tip of the fiber. When the microsphere moves due to contact with the surface being measured, changes in the scattered light can be monitored, thereby detecting the displacement of the microsphere. In 2012, Xin et al. used conical probe fiber optical tweezers to achieve optical capture, driving, and arrangement of particles [70]. By adjusting the laser power, they precisely controlled the movement distance of silica particles with a diameter of 3 mm and successfully arranged the particles into hexagonal, triangular, and other two-dimensional patterns. In addition to using ordinary single-mode fibers, single-fiber optical tweezers systems can also achieve more functions by expanding the degrees of freedom of light in the fiber. Apart from having a larger core diameter and providing greater capture power [72], the modes supported for light transmission in multimode fibers can also serve as a degree of freedom to expand the functions of optical tweezers. In 2015, Liu et al. [73] separated the LP01 and LP11 modes in a few-mode fiber using a mode selector and designed the fiber tip into a special conical shape to guide the LP11 mode beam to focus and generate a large convergence angle, thereby generating optical capture force. At the same time, the LP01 mode beam is not focused and produces a scattering force, which is used to push the microparticles away from the fiber tip. The mode selector is used to adjust the power of the LP01 and LP11 mode beams to control the optical force required for capturing and emitting microparticles. By changing the settings of the mode selector, the power of the LP01 mode beam can be suddenly increased while simultaneously reducing the power of the LP11 mode beam, thereby changing the nature of the optical force and achieving particle emission, as shown by Fig. 2d.

In addition to different modes producing different forces, light of different wavelengths can also produce similar effects. In 2015, Liu et al. used two wavelengths of light to independently control the capture and emission of target microspheres [74]. The 980 nm laser beam captures the target polystyrene microspheres by shaping the fiber tip into a special conical shape, while the 1480 nm laser beam emits the captured polystyrene microspheres through the thermophoretic force generated by the thermal effect, as shown by Fig. 2e. To date, single-fiber optical tweezers technology continues to innovate in manipulation techniques. Designing special fiber probe tips not only promotes laser focusing to enhance the localization of the optical field and provide greater capture force but can also be combined

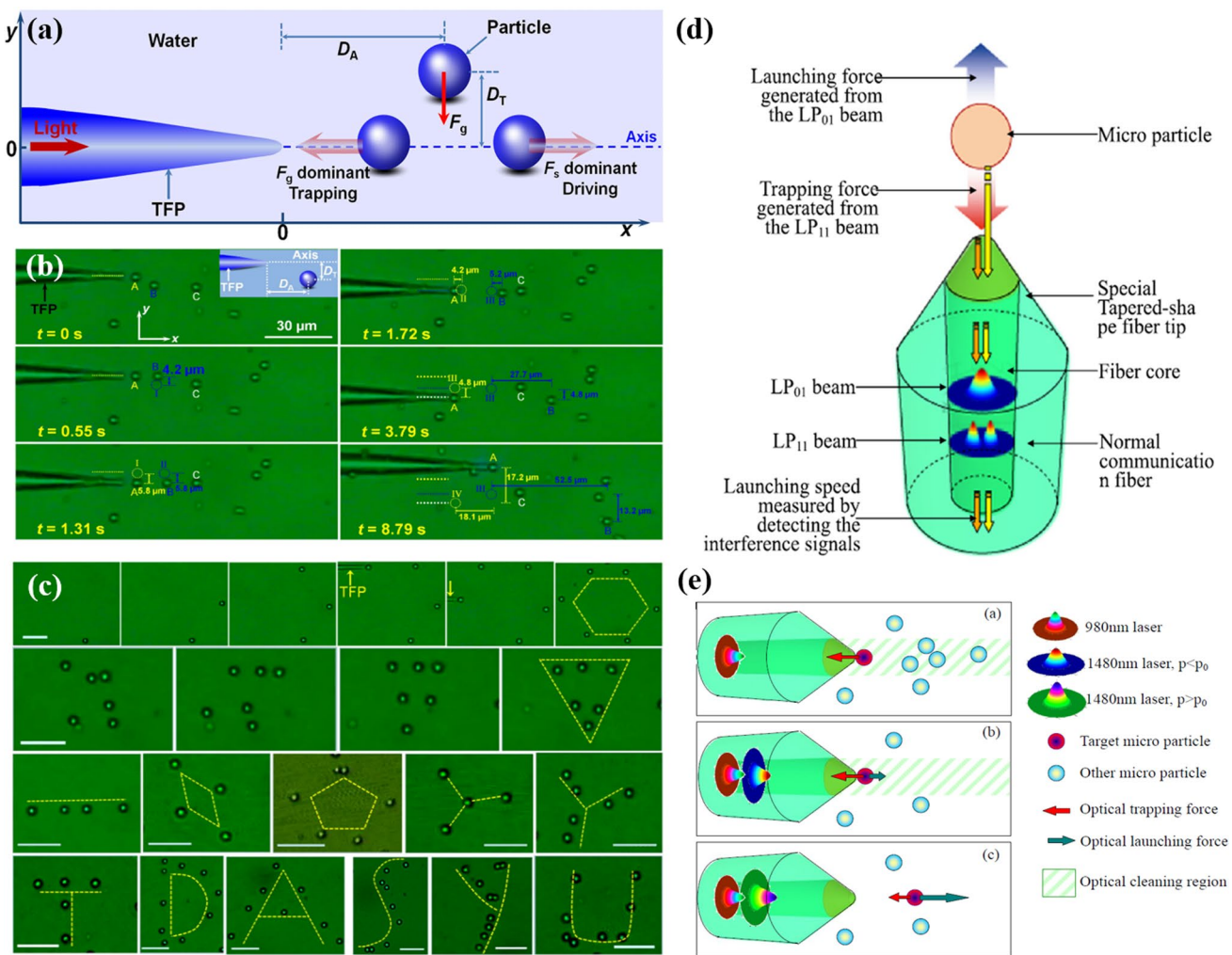


Fig. 2 **a** Schematic diagram of a tapered fiber probe (TFP) operating a particle [70]. **b** Capture and drive a series of optical microscope images of particles using TFP [70]. **c** The ability to precisely arrange particles to form specific patterns using TFP [70]. **d** The role of LP₁₁ mode beam and LP₀₁ mode beam at the fiber tip, and how to measure the emission characteristics of particles by detecting interference signals. These interference signals are generated by backscattered light on the surface of the particle and the end of the fiber. By analyzing these signals, the velocity, acceleration and travel distance of the particle during the emission process can be calculated [73]. **e** Working principle of dual wavelength single fiber optical tweezers. Including how to control the capture, emission and cleaning of particles by adjusting the power of the two laser beams [74]

with structured light to form photonic hooks, accomplishing the task of manipulating particles around obstacles [75]. The optical field generated by the photonic hook can vary along a curve to bypass obstacles and manipulate particles from different angles. To generate a photonic hook, the tip of the fiber probe needs to be designed into an asymmetric shape, considering the geometric parameters of the fiber probe, such as the truncation angle (α), cone angle (β), and diameter (d), to complete the design of the focal length, tilt angle, and optical field strength of the photonic hook, as shown by Fig. 3a. Figure 3b shows that the photonic hook can bypass multiple cells in front of the fiber probe tip, selectively capturing and manipulating a single red blood cell. At $t = 15\text{ s}$, a red blood cell (labeled A) is stably captured, while other red blood cells (labeled B) remain in place. When the truncated fiber probe moves downward, the captured red blood cell A moves with it, while red blood cell B remains nearly stationary. This indicates that the photonic hook can manipulate the captured cell to move along a specific path. The aforementioned single-fiber and dual-fiber optical tweezers both utilize optical forces generated by focused light to control the motion of particles, and thus are limited by the diffraction limit when manipulating particles of smaller scales. Compared to traditional far-field optical tweezers based on single-beam gradient force, near-field optical tweezers overcome the limitations of optical resolution diffraction limit, thermal effects, and many other factors, enabling the capture and manipulation of nanoscale microparticles. When light propagates in an optical fiber, total internal reflection occurs.

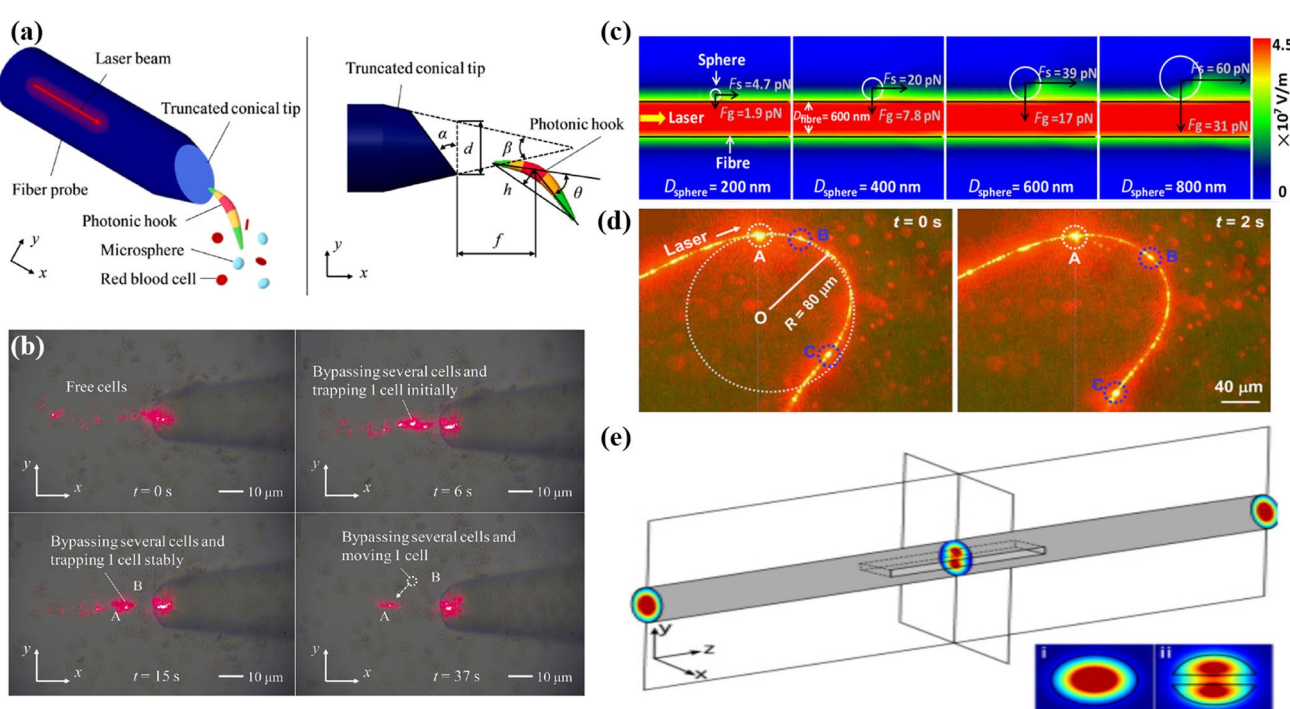


Fig. 3 **a** Schematic diagram of photonic hook capturing multiple particles and geometric definition of truncated conical probe tip. This illustrates how photonic hook technology can exploit the specific geometry of a fiber probe to enable selective capture and manipulation of individual particles. By adjusting the shape and angle of the probe tip, the characteristics of the photon hook can be controlled to precisely manipulate the target particles [75]. **b** A series of light microscopy images of individual red blood cells captured and manipulated using a photonic hook with a truncated conical probe tip demonstrates the ability of photon hook technology to capture and manipulate individual red blood cells [75]. **c** Simulations of the longitudinal electric field distribution of polystyrene spheres of different diameters when captured at a distance of 20 nm from the surface of the fiber are shown. These images show the distribution of the electric field in the vicinity of the fiber with spheres of different sizes when the fiber is 600 nm in diameter [76]. **d** Three nanospheres (labeled A, B, and C) are shown to be captured by nanofibers. These nanospheres are captured by 650 nm red light and are transmitted along the fiber due to the scattering force of the evanescent field around the fiber [77]. **e** A cross-section of a tapered fiber with a slot is shown, which includes the fiber base mode (labeled I) on both sides of the groove area and the tapered fiber base mode with a groove in the center (labeled II). This illustrates how the mode transition of the fiber pattern in the center of the slot area changes from the fiber base mode to the base mode of a tapered fiber with a slot and back again [78]

In this case, the light does not penetrate the boundary but generates an evanescent field near the interface. This field decays rapidly in the direction perpendicular to the interface, usually within a range of a few hundred nanometers to a few micrometers. When particles are placed within the evanescent field region, they are simultaneously acted upon by the gradient force and scattering force of the optical field. The gradient force pulls the particles towards regions of higher optical intensity, while the scattering force pushes the particles along the propagation direction of the light. Figure shows the simulated longitudinal electric field distribution of polystyrene spheres of different diameters captured at a distance of 20 nm from the surface of a 600 nm diameter fiber, as well as the calculated optical gradient force and scattering force. As the sphere diameter increases, the gradient force and scattering force caused by the evanescent wave field around the fiber also increase, indicating that larger spheres can be more easily captured and transported faster [76], as shown by Fig. 3c. Due to the adhesive gradient force of the fiber on the particles, bending the fiber can also change the transmission path of the particles [77], as shown by Fig. 3d. In addition, evanescent field-based optical fiber tweezers can enhance optical capture capability by introducing physical asymmetry through slot structures [78], as shown by Fig. 3e. As shown in the figure, the intensity of the evanescent field in the slot region of the slotted waveguide fiber is much higher than in other regions of the fiber. By controlling the polarization direction of the incident light, the optical field intensity in the slot region can be further modulated. When the polarization direction of the light is perpendicular to the slot wall, due to the discontinuity of the electric field at the medium boundary, more optical field energy can exist outside the waveguide, thereby generating a stronger optical field in the slot region. By propagating light in two opposite directions to form a standing wave, the intensity of the optical field can be further enhanced. The standing wave mode produces a periodic optical intensity distribution in the slot

region, providing additional longitudinal confinement force for the particles and enhancing the capture stability. Ultimately, low-refractive-index nanoparticles can be captured at optical powers as low as 1.2 mW.

In summary, single-fiber and dual-fiber optical tweezers each have their unique advantages and application areas. With the development of micro-nano fabrication technology, optical fiber tweezers can be further miniaturized and integrated onto chips to achieve portable and low-cost optical manipulation platforms. Compared to dual-fiber optical tweezers, single-fiber optical tweezers only require one fiber, have a simpler structure, are easier to bend and manipulate, and are suitable for use in complex or narrow spaces, improving flexibility and portability. Using a single fiber helps reduce interference between fibers and improves the stability and capture accuracy of the system. Furthermore, single-fiber optical tweezers can adjust the capture position by changing the laser wavelength, providing more degrees of freedom for manipulation. Single-fiber optical tweezers are simpler in design, lower in cost, and have higher flexibility, making them advantageous in many application fields, especially when portability and integration are required. For example, they can be applied in biomedicine for cell manipulation, drug delivery, and single-cell analysis to reduce interference with biological samples, or in optical sensing for precise measurement of force and displacement, or in environmental monitoring for capturing and analyzing microparticles in the air, or in materials science for studying the mechanical properties of materials, or in quantum optics for capturing and manipulating single atoms or quantum dots, providing new tools for quantum information processing. Combined with machine learning and artificial intelligence technologies, single-fiber optical tweezers can achieve automation and intelligence in optical manipulation, improving the precision and efficiency of manipulation.

2.2.3 Fiber optical tweezers based on special fiber cores

To enhance the capture capability of optical fiber tweezers for microparticles, designing special conical fiber probes at the end of conventional single-mode or multimode fibers alone cannot meet the requirements for more precise manipulation. Therefore, optical fibers that can generate stronger optical trapping forces are needed to manipulate different microparticles. Among them, designing heterogeneous optical fibers suitable for specific environments or applications has significantly improved manipulation performance compared to using conventional fibers. The core of conventional fibers is only distributed along the central axis of the cladding, forming a concentric circle structure with the cladding cross-section. By changing the shape of the core and cladding, varying the position of the core, and creating holes in the cladding, special-core fibers can be roughly divided into multi-core fibers, off-center core fibers, and ring-core fibers according to the shape of the core [79], as shown by Fig. 4a. These structures can provide different optical field control capabilities, not only better regulating the spatial distribution of the output optical field but also generating a stronger evanescent field on the fiber surface as the core is closer to the cladding surface, which is conducive to near-field capture. In 2003, Taylor et al. fabricated a conical structure from a high-GeO₂-doped single-mode fiber through selective chemical etching, with a hollow tip and metallization treatment. This design enables the fiber probe tip to generate an annular light distribution for capturing microparticles [80], as shown by Fig. 4c. The annular light distribution generated by this hollow-tipped fiber can provide lateral confinement force, and by adjusting the size of the annular aperture, it can match target microparticles of different sizes, achieving three-dimensional capture. In 2008, Yuan et al. used a dual-core fiber and manufactured a tapered conical dual-core fiber probe through heating and stretching, forming a small hemispherical high-numerical-aperture microlens at the fiber tip, successfully capturing yeast cells at an optical power of 5 mW [81], as shown by Fig. 4b. At the same optical power, the capture force was more than 3 times stronger than that of a single-mode fiber. In 2014, Zhang et al. spliced a conventional 980 nm single-mode fiber with a standard single-mode fiber and applied a certain offset (about 2 microns) to excite the LP11 mode beam [82]. By changing the optical field distribution of the LP11 mode beam, i.e., the direction of the transverse optical field distribution and the power ratio of the two lobes, the deflection and orientation of yeast cells can be achieved. By changing the ratio of the light intensity distribution of the LP01 and LP11 modes and twisting the fiber to change the field mode direction of the LP11 mode beam, the manipulation of yeast cells can be realized. In 2016, Zhang et al. designed an optical fiber tweezers based on an elliptical-core fiber [83], as shown by Fig. 4d. This elliptical-core fiber can excite and stably transmit the LP11 mode beam when using a 980 nm wavelength light source, simplifying the experimental setup based on the 2014 results. Similarly, the rotation of the captured microparticles can be achieved by rotating the tip of the elliptical-core fiber, with the rotation angle being the same as that of the fiber tip.

With the development of mode division multiplexing technology, different independent optical modes can be transmitted and controlled in a single fiber, enabling optical tweezers systems to simultaneously generate multiple independently controllable optical traps. Different modes can form more complex and precise optical field distributions in

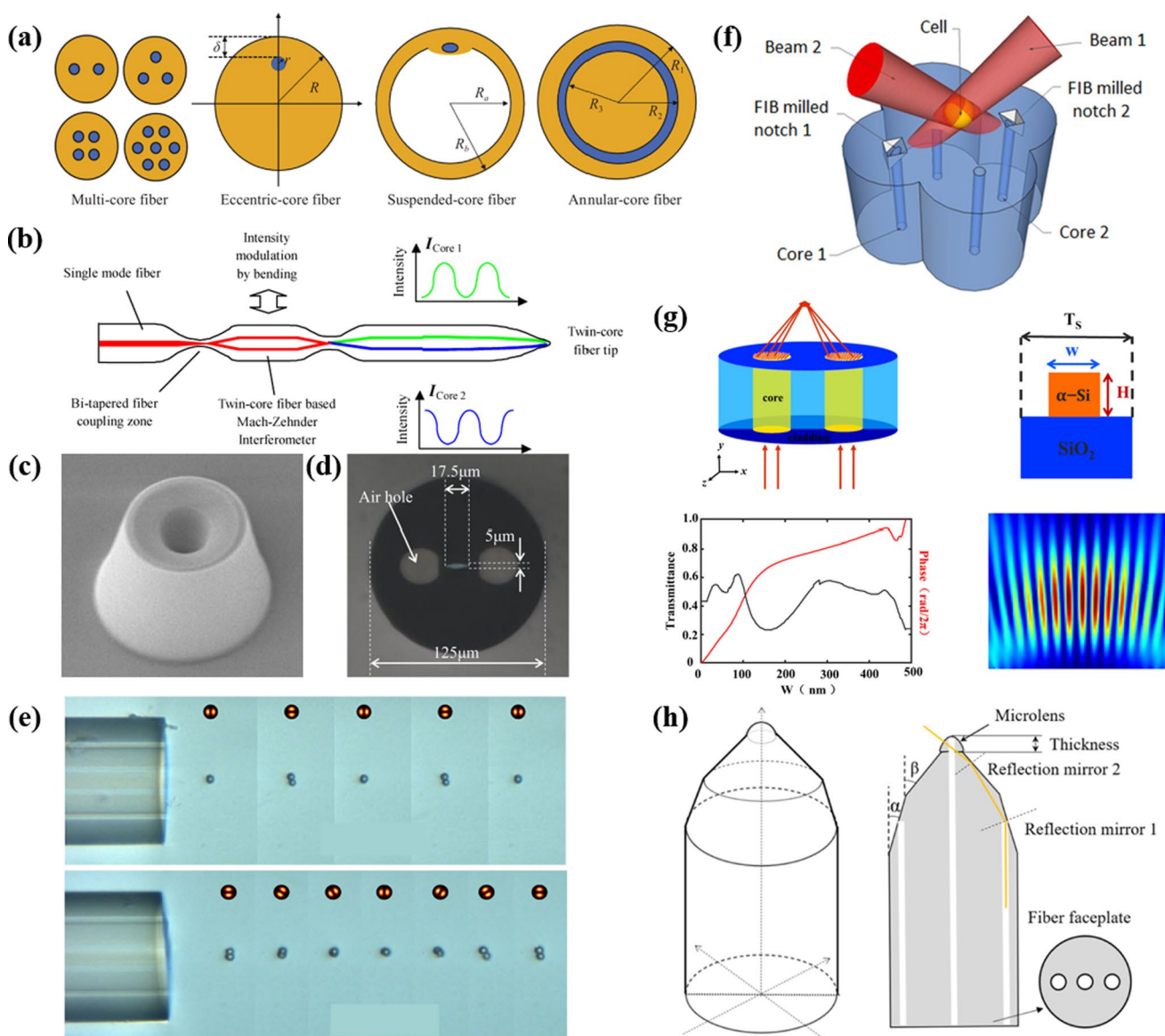


Fig. 4 **a** Schematic diagram of cross-section of common special core fibers [79]. **b** It shows how to control the direction of the trapped particles by integrating a Mach-Zehnder interferometer in a twinax fiber. By adjusting the interferometer, the intensity of light in the two fiber cores can be changed, which affects the beam output from the tip of the twinax fiber, enabling precise manipulation of the particles. This configuration allows the dual-core fiber optical tweezers to not only capture the particles, but also control the direction of the particles [81]. **c** A selectively chemically etched, tapered fiber probe tip with a central void area [80]. **d** Cross-section of an elliptical core fiber [83]. **e** Experimental results of particle manipulation using photonic lanterns (PL) and few-mode fibers (FMF). By switching between two degenerate LP11 modes, a 90° rotation of the particles can be achieved. This is because two fibers that generate the LP11 mode are connected to the output of the polarization beam splitter (PBS), which changes the polarization state through the polarization synthesizer to switch between the LP11a and LP11b modes to achieve particle displacement. Once the two particles are trapped, they can be rotated continuously by changing the direction of the linear polarization state [84]. **f** Multi-core fiber tweezers work by processing mirrors on the end face of the fiber so that the beams are reflected and converged at specific angles, creating a capture area [85]. **g** The design and operating principle of the tweezers for twinax fibers, including their basic structure, cell structure, transmission and phase characteristics, and the interference pattern formed by the two beams [86]. **h** The structure of a three-core fiber, i.e., the key parameters include the fiber core radius, tapered fiber length, the distance between cores, the core diameter, and the thickness of the microlens [87]

three-dimensional space, enhancing the throughput and efficiency of optical tweezers systems. Different modes can carry different angular momentum information, providing optical tweezers with new manipulation degrees of freedom such as rotation and twisting, which helps achieve more complex particle manipulation. For example, using a photonic lantern to excite LP01 and LP11 modes, where the LP01 mode is used to capture a single microparticle, while the LP11 mode has two lobes and can simultaneously capture two smaller microparticles [84]. As shown in the Fig. 4e, by changing the

polarization state in the polarization synthesizer, switching between the two polarization modes of LP11 can be achieved, realizing the displacement of microparticles. By continuously rotating the linear polarization state of the input signal, continuous rotation of microparticles can be achieved. With the development of spatial light modulation technology and advancements in fiber manufacturing processes, multi-core fiber technology in the field of optical communication has also progressed rapidly. Firstly, the multi-core structure can avoid using multiple independent fibers, simplifying the complexity of the optical path system, reducing the occupied space, and improving the stability of the system. Secondly, multi-core fibers can achieve the transmission of multiple independent beams in a single fiber, with each core being independently controllable, realizing simultaneous manipulation of multiple capture points, greatly improving the parallel processing capability of the system compared to single-mode fibers. Furthermore, by controlling the phase and intensity of different cores, complex optical field distributions can be achieved, capable of generating various optical trapping modes such as multi-beam arrays and vortex beams, thereby providing more precise and dynamic particle manipulation capabilities. Rong et al. employed a seven-core fiber optical tweezers and successfully captured, pushed, and rotated *Escherichia coli* by exciting higher-order modes [88]. Anastasiadi et al. used focused ion beam (FIB) milling technology to fabricate reflectors on the cores along two diagonals of a multi-core fiber, forming a stable three-dimensional optical trap [85], as shown by Fig. 4f. The maximum NA of the optical fiber tweezers was 1.039, capable of generating a maximum capture force of 26.5 pN, successfully capturing yeast cells with a diameter of 7 microns stably in three-dimensional space, and obtaining spectra of live and dead cells under a Raman probe. Zhang et al. designed an optical trajectory transport device using a three-core fiber [89], utilizing a light optical model method based on spatially resolved geometry to calculate the capture force of the beam on microparticles, analyzing the reflection and refraction of the beam on the microparticles, as well as the resulting gradient force and scattering force. By adjusting the optical power of each core in the three-core fiber, different trajectories can be formed, causing the microparticles to move along these trajectories. The device has potential applications in drug delivery, targeted therapy, and microparticle characterization analysis.

In recent years, with the continuous improvement of fiber end-face processing technology and the emergence of new fiber structures, driven by the integration of micro-nano technology and fiber technology, the integrated development of fibers and microstructures has become a new trend to enhance the performance of special-core fiber optical tweezers in practical applications. For example, Liu et al. integrated a metasurface on the end face of a dual-core fiber, causing the beams emitted from the two cores to deflect and converge in the far field, forming interference fringes and achieving multi-point optical capture [86], as shown by Fig. 4g. Zhu et al. designed a three-core fiber optical tweezer probe with a dual-cone angle and a micro-lens at the tip, realizing non-contact capture through the superposition of the optical fields emitted from the central core and the two side cores [87], as shown by Fig. 4h. The dual-cone angle and micro-lens structure at the tip help control the optical field distribution and focusing effect more precisely, thus improving the capture efficiency and accuracy. By utilizing the difference in input optical power of different cores in the three-core fiber, the distribution of the optical field can be controlled through mode interference, and this multi-core collaborative working mode improves the manipulation and flexibility of the optical tweezers.

In summary, special-core fibers have stronger optical field control capabilities, superior optical performance, and higher system integration compared to ordinary fibers, and can be widely applied in biomedical, micro-nano fabrication, quantum manipulation, and other fields, with broad development prospects in the field of optical fiber tweezers. However, the current development of special-core fibers still needs to address issues in manufacturing technology, such as higher-precision manufacturing processes, higher-precision optical field control capabilities, and how to improve system stability. Future developments in optical fiber tweezers can be designed by integrating new micro-nano structures, optimizing multi-core structures, integrating sensing, spectral analysis, and imaging functions, as well as developing in the direction of intelligence.

2.3 Metamaterial optical tweezers

With the rapid development of the field of optical micromanipulation, the shortcomings of traditional optical tweezer systems such as large size, single function, and high energy consumption have become obstacles. As a new type of optical material, metamaterials have powerful functions for multi-dimensional control of light field strength, polarization, and phase. At the same time, metasurfaces and metalenses made of metamaterials also have the advantages of miniaturization, integration [90] and multi-function [91, 92]. By applying metamaterials to the optical tweezer system, the size of the system can be greatly reduced, the types and sizes of controllable particles can be widely broadened, the power of the incident laser can be reduced, and even the trajectory programming of controllable particles can be realized.

In this section, we will review and discuss the latest achievements of metamaterials in the field of optical tweezers in recent years, and clarify their potential in the future development of nanophotonics.

2.3.1 Plasmonic tweezers

Extending the capture range of optical tweezers systems from the micro-scale to the nano-scale opens up unprecedented opportunities for many scientific fields, allowing precise manipulation of individual particles at the nanoscale. Among the possible options, metal metamaterials stand out for their extraordinary optical response at subwavelength scales, and their operating principles are mainly based on surface plasmonic polaritons (SPPs). These plasmons are surface charge oscillations caused by the interaction of metal nanostructures with conductive electrons when exposed to light. When a metal nanostructure is irradiated with light, the free electrons in it are excited, forming oscillations. At a specific frequency, the oscillations of these electrons resonate with the electromagnetic waves of the incident light, causing a strong electron cloud oscillation, a specific phenomenon known as "surface plasmon resonance (SPR)". Thanks to these SPPs, when light hits a metal nanostructure, it forms a highly concentrated local electromagnetic field on the surface of the structure, which is much stronger than the incident light and has a great intensity gradient. Using this local electromagnetic field, it is possible to generate an optical force sufficient to manipulate nanoscale particles. In 2013, Min et al. proposed a variant of plasmonic tweezers based on radially polarized beam-excited metal thin films, as shown in Fig. 5a [93]. It has the effect of attracting and trapping both Rayleigh particles and Mie particles, and the capture of Mie particles is still successful. Unlike the dominant scattering force in the traditional optical tweezers, the net force used to trap the particles in the plasmonic tweezers is composed of the strong gradient force generated by the coupling of the greatly enhanced SPP field and the metal particles, and the anomalously weak scattering force caused by the thrust exerted by the focused SPP propagation. The key to this lies in the strongly focused SPP field. Subsequently, in 2019, Samadi et al. prepared a hexagonal golden triangle array by angle-resolved nanosphere etching, and used this structure to capture PS nanospheres with a diameter of 650 nm, proving that it can be used as plasmon optical tweezers with controllable operating wavelengths and high capture efficiency [94]. At the same time, it is shown that under the incidence of 1064 nm wavelength, the capture stiffness of the optical tweezers can be effectively adjusted by SPP force, such as Fig. 5b. In a hexagonal golden triangle array, there is no gap band pattern between adjacent golden triangles, and their backscattering fields can be superimposed on each other to bind particles to the center of the hexagonal array. At the same time,

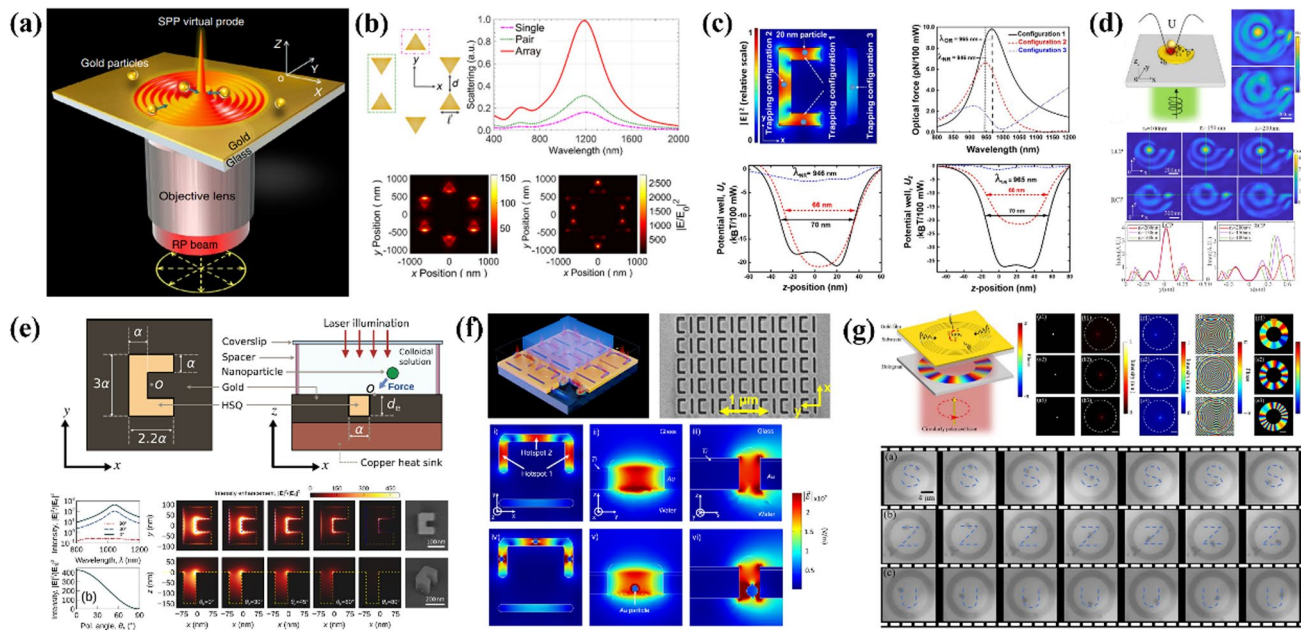


Fig. 5 plasmonic tweezers. **a** Plasmonic tweezer variant based on strong gradient force[93]. **b** Hexagonal Golden Triangle Array Optical Tweezers[94]. **c** Nano-sorting based on asymmetric split resonant rings[95]. **d** Nano-sorting based on Archimedes helical structure[96]. **e** Plasmonic optical tweezers that can be dynamically adjusted[97]. **f** SIBA-based plasmonic tweezer[98]. **g** Particle trajectory programming based on concentric ring structure[99]

due to its three-dimensional in-plane intrinsic orientation, the excitation of the surface plasmon is less dependent on the polarization of the incident light.

Plasmonic tweezers can also be used as an effective nanoscale sorting tool. In 2021, Kotsifaki et al. achieved sequential capture of PS nanospheres with a diameter of 20 nm by etching an asymmetric split ring resonator on a gold thin film, as shown by Fig. 5c, and demonstrated that the structure can be used as a light-driven nano-sorting device under the excitation of a low-power laser, providing an alternative method for simultaneously capturing multiple particles at different hot spots [95]. By manipulating the opening and closing of the incident laser light, combined with the Brownian motion of the trapped particles, they can sequentially move to adjacent plasmon hotspots (i.e., capture sites) to achieve mass transport at the nanoscale. The introduction of introducible structures is also a common means to achieve nano-sorting. As Fig. 5d shows that in 2023, Liu et al. designed a plasmonic tweezer with an Archimedean helix structure to achieve spatiotemporal separation of nanoparticles [96]. Based on the spin-orbit interaction of circularly polarized light, the scattered light of the incident circularly polarized light along the Archimedes helix will produce high-quality plasmon hotspots on the metal disc when the chirality is the same. They exploit circularly polarized light incidences with different spins to produce focused fields and imperfect vortices, respectively. Therefore, by switching the spin of the incident light, the sorting of nanoparticles in the time domain can be realized. At the same time, the spatial sorting of nanoparticles can be realized by using multiple Archimedes helix structures with different chirality to form an array. They also used a 532 nm laser incidence and demonstrated the extraordinary sorting capability of this structure through numerical simulations.

At the same time, based on the characteristics of plasmons that can generate local strong electric fields, plasmon optical tweezers can effectively reduce the power of incident light, which will greatly reduce the thermal effect on the manipulated object, and provide it with the possibility of manipulating fragile objects. In 2022, Zaman et al. realized a dynamically tunable plasmonic optical tweezer such as Fig. 5e [97]. The polarization sensitivity of the C-shaped structure is used to dynamically control the electromagnetic field and the associated trapping force, which allows the capture state of the particles to be maintained at low field strengths. At the same time, due to the engraving of the C-shaped groove on the gold film and the filling of HSQ (hydrogen silsesquioxane) in it, it adopts a reflective mode and is not limited by the transparent substrate of the C-shaped hole. They used 1064 nm laser excitation to generate a tightly focused focus when the structure generates plasmon resonance, which is characterized by a fleeting field, thus generating a strong gradient force to achieve particle capture. By changing the polarization angle of the incident light, the amount of the capture force can be dynamically adjusted, so that the capture state can be maintained with a small field strength. In 2023, Boulumis et al. used focused ion beam milling (FIB) etching thin gold films to form an array of metamaterials, generating self-induced back-action (SIBA) in the structure, reducing the laser power and increasing the capture stiffness of optical tweezers, as shown in Fig. 5f [98]. At low excitation intensities, an optical trap with a stiffness of 4.18 ± 0.2 (fN/nm)/(mW/ μm^2) was generated, and stable capture of gold particles with a diameter of 20 nm was achieved. They used plasma cavity resonance tuning to allow the particles to dynamically reconstruct the intensity in the cavity while being trapped, and this optical coupling helped reduce the laser power. With proper structural design, the synergistic effect of SIBA and Fano resonance is used to produce a strong photomechanical response, thereby facilitating long-term optical capture at low laser power.

In addition, since the hot spot of the SPP field is not limited to the predefined local nanostructures, the plasmon optical tweezers can be optically programmed, allowing for free manipulation of the particles. More recently, in September 2024, Wang et al. designed a gold thin film with concentric ring slits and proposed a novel plasmon optical tweezer system for dynamic manipulation of gold particles by customizing tunable SPP fields, such as Fig. 5g [99]. It has an editable plasma hotspot that enables stable capture and dragging of gold particles, enabling its manipulation along a specific trajectory in the SPP field. They used nano-rings in the structure to excite the SPP field, and multiple concentric rings could significantly enhance the strength of the SPP field, thereby stably trapping gold particles. At the same time, by loading the designed hologram onto the spatial light modulator (SLM), the excited SPP field can be modulated, so that the hot spots of the excited SPP field can be programmed to realize the specific trajectory manipulation of gold particles. In combination with plasmons, many powerful new optical tweezers have emerged, which will greatly enrich the diversity of the field of optical micromanipulation.

2.3.2 Metasurface tweezers

Metasurfaces are widely used in optical systems, such as optical tweezers and optical spanner, due to their powerful ability to manipulate the light field and the advantages of miniaturization and integration of the body[100–103]. Optical tweezers rely on a highly focused laser beam, and when the target particle is near the focal point of the beam, the

scattering force and the light intensity gradient force reach equilibrium, and the particle will be stably captured at the focal point. However, this often requires a bulky optical system. Through the application of metasurfaces, it is possible to greatly reduce the volume of the objective lens used for focusing and improve the accuracy and number of particles while retaining the basic functions of traditional optical tweezers. In 2018, Markovich et al. implemented a bifocal lens for orthogonal linearly polarized light using metal nano-antennas containing overlapping longitudinal, transverse, and crossed metal nano-antennas, as shown in Fig. 6a [104]. By changing the linear polarization state of the incident light, the micron-sized polystyrene microspheres can be continuously transferred between the two focal points, and the optical capture stiffness of the two focal points is quantitatively analyzed by using the particle tracing algorithm. In 2020, Chantakit et al. designed and experimentally validated an amorphous silicon-based geometric phase metasurface for two-dimensional optical capture operations in the near-infrared band, such as Fig. 6b [105]. Due to their compact size, these metasurfaces offer significant flexibility for fine-tuning and alignment of optical traps. Using this lens, the research team used a metasurface with NA = 0.6 to perform two-dimensional particle manipulation and successfully achieved a META-shaped arrangement of polystyrene (PS) particles suspended in water. In order to solve the influence of large chromatic aberration on the focusing ability of metasurfaces, and further improve the focusing ability. As shown in Fig. 6c, in 2022, Wang et al. proposed a novel metasurface optical tweezers based on a particle group optimization algorithm, which achieved broadband achromatic aberration of metasurfaces with a bandwidth of 100 nm under incidence in the 1014–1114 nm band [106]. At the same time, its high numerical aperture is as high as 0.97 and the focusing efficiency is 0.44. Compared to dispersive metals, it can maintain the constancy of the optical force, the motion state of the trapped particles, and the stability of the capture position, improving the effect of wavelength bandwidth. This enables stable three-dimensional capture of silica particles up to 350 nm in diameter. The particle swarm optimization algorithm is used to adjust the phase distribution of the metasurface to meet the phase compensation required by different wavelengths, so as to achieve broadband achromatic. At the same time, the higher NA value in turn enhances the optical force generated by the focusing and the capture efficiency, which promotes the stable capture and manipulation of silica particles.

In addition, the use of metasurfaces makes it possible to accurately capture and manipulate multiple particles at the same time. Recently, in March 2024, Yu et al. reported a compact on-chip multi-trap optical tweezers based on guided

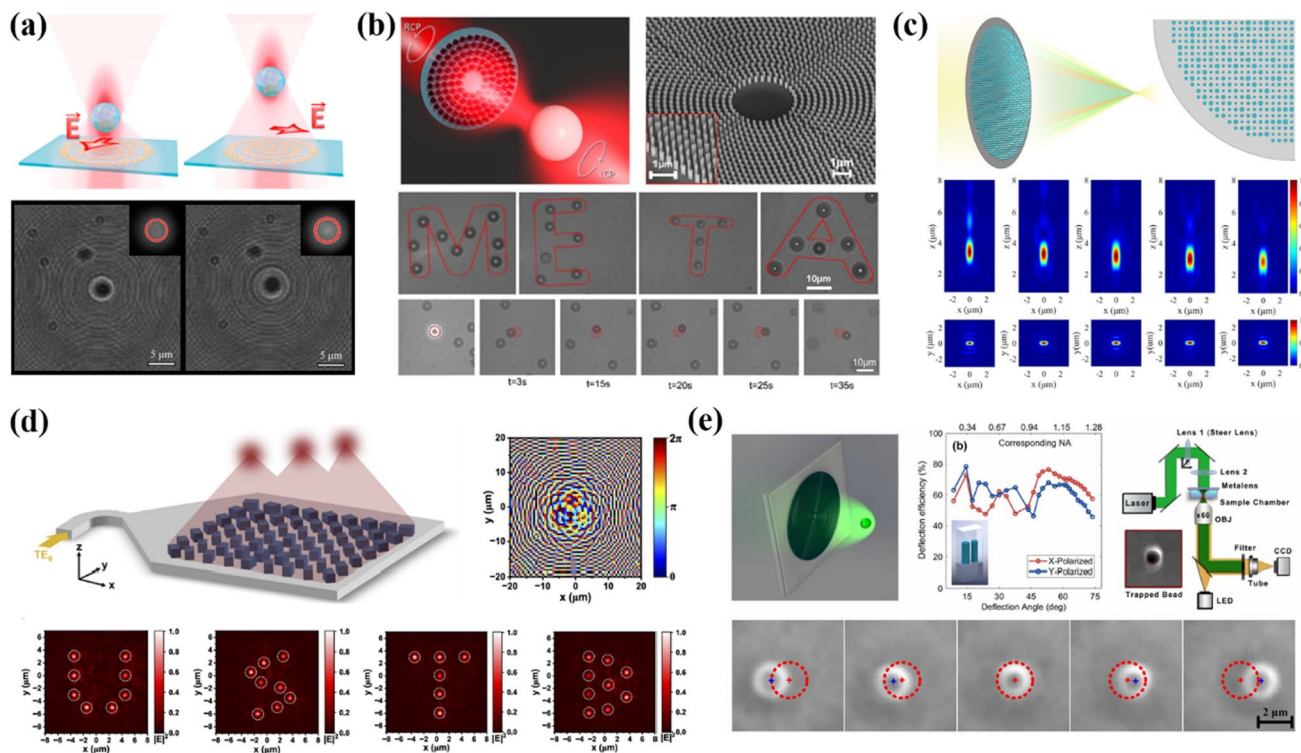


Fig. 6 metalens optical tweezers. **a** Polarization-sensitive bifocal metalens optical tweezers[104]. **b** Optical tweezers for metalenses based on geometric phase[105]. **c** Achromatic metalens optical tweezers based on Particle Swarm Optimization (PSO) algorithm[106]. **d** Wave-guide-driven on-chip multi-trap metalens optical tweezers[107]. **e** Water-immersion transmission and polarization-insensitive metalens optical tweezers with high capture stiffness[108]

wave-driven metasurfaces, which have an effective NA value of up to 0.88 and can simultaneously manipulate three PS particles with a radius of 150 nm, such as shown in Fig. 6d [107]. They proposed an analytical design method to generate multiple focal points according to demand in the free space outside the chip, and experimentally implemented a capture pattern of the letters U" S" T "B" using PS particles. By rotating the angle of the silicon nanometer on the metalens, the metaatomic library is constructed to realize the arbitrary phase modulation of the scattered light wavefront, and then manipulate the scattered light coupled to the waveguide to form a multifocal in the far field. In the same year, in order to improve the accuracy and stability of the capturing of metalens optical tweezers, Yang et al. designed a transmissive polarization-insensitive water immersion metalens optical tweezers, such as Fig. 6e [108]. It has an ultra-high NA value and a focusing efficiency of 1.28 and about 50%, respectively. At the same time, it has the same order of magnitude of transverse capture stiffness as conventional optical tweezers, exceeding 500 pN/(μmW). And because of the inherent stability of the overall structure, it can be guaranteed that the capture position will not drift. Experimentally, the stable capture of polystyrene particles with a diameter of 1.76 μm and optical manipulation in the range of 2 μm were achieved when the 532 nm laser was incidence. The metalens is based on a metagrating composed of appropriate nanoantenna arrays, which has a large-angle and high-efficiency deflection effect on the incident light, so that it can produce a continuous full 2π phase gradient for the incident light of arbitrary linear polarization, so that the metalens has a very high NA value and is not sensitive to polarization. It can be seen that the metasurfaces optical tweezers technology can not only greatly reduce the volume of the optical tweezers system, but also have the advantages of stable operation, diverse functions, and easy integration, which has laid a solid foundation for the wide application of optical tweezers in the future.

This section focuses on the frontier progress of metasurfaces tweezers and elucidates their important role in the field of micro-nano optics. However, in addition to optical tweezers, optical spanner is also one of the extraordinary applications of metasurfaces[109, 110], which can generate specific optical vortices in the focal plane by manipulating the spin angular momentum (SAM) and orbital angular momentum (OAM) of the incident light[111, 112], and realize the rotational manipulation of particles. In combination with the phase gradient, it is possible to achieve fully control of particles in two-dimensional[113]. In addition, it can also be used in drug delivery, particle sorting and other fields, such as the "optical conveyor belt" recently proposed by Gao et al. has this function[114]. Since this section mainly focuses on the discussion of metasurfaces tweezers, we will not introduce more about optical spanner.

Eventually, we will compare the performance of fiber optical tweezers and metamaterial optical tweezers, which will intuitively reflect the relative strengths and weaknesses (Table 1).

3 Applications based on nanophotonics

3.1 Optical manipulation in cells

The ability to precisely manipulate individual cells and study their properties and interactions is crucial for understanding fundamental biological processes and developing new applications in areas such as cell biology, biophysics, and biotechnology. In recent years, optical methods have emerged as powerful tools for non-contact, non-invasive manipulation of cells with high spatial and temporal resolution. Light-based techniques exploit the interaction of focused light with matter to generate forces and torques that can be used to trap, move, deform, or stimulate cells. The most well-known and widely used optical manipulation technique is optical tweezers, which use a tightly focused laser beam to create a three-dimensional trap for cells and other small objects. Since their invention by Arthur Ashkin in the 1980s, optical tweezers have found numerous applications in cell biology, from isolating single cells and measuring their mechanical properties to studying cell-cell interactions and intracellular processes. In addition to optical tweezers, other optical manipulation methods have been developed to expand the capabilities and address the limitations of single-beam traps. These include holographic optical tweezers that use spatial light modulators to create multiple traps and manipulate many cells simultaneously, and plasmonic tweezers that utilize localized surface plasmons to generate strong trapping forces with low laser powers. Optical stretchers and optofluidic devices have also been used to deform and analyze cells in microfluidic environments. Despite the remarkable progress, optical manipulation of cells still faces challenges and limitations. Photodamage to cells from prolonged exposure to high laser intensities remains a concern, especially for sensitive cell types or applications requiring long-term manipulation. The small trapping forces generated by optical tweezers limit their ability to manipulate large or strongly refractive cells, while the diffraction-limited nature of focused light beams restricts the spatial resolution and precision of optical traps.

Table 1 Comparison between fiber optical tweezers and metamaterial optical tweezers

Performance metrics	Fiber optical tweezers	Metamaterial optical tweezers
Manipulation force magnitude	Dual-fiber optical tweezers: Generate significant capture forces with wide capture ranges at focal points, suitable for manipulating larger particles and cells. Single-fiber optical tweezers: Provide precise control over smaller particles through gradient and scattering forces	Plasmonic tweezers: Utilize strong gradient forces from enhanced SPP fields for nanoscale particle manipulation, ideal for high-precision applications.
Positional precision	Can achieve precise control of particle position and motion by adjusting the laser power and fiber position	Metasurface tweezers: Offer programmable force landscapes through structured light, enabling dynamic control over particle trajectories
Operational stability	Dual-fiber optical tweezers: Exhibit high stability with stable equilibrium points. Single-fiber optical tweezers: Offer stable operation in various environments	Plasmonic tweezers: Provide nanoscale precision due to localized SPP fields.
Fabrication complexity	Ordinary fiber tweezers: Relatively simple fabrication process Special-core fiber tweezers: Higher fabrication complexity, requiring precise control of fiber structure and dimensions	Metasurface tweezers: Enable precise manipulation through holographic optical tweezers and other advanced techniques
Integration potential	Easy to integrate into microfluidic channels or photonic chips due to their small size	Stability depends on the consistency of the field and the structural stability of the nanostructures
Applications	Cell manipulation, particle sorting, <i>in vivo</i> trapping	Plasmonic tweezers: High fabrication complexity, requiring nanoscale precision in fabricating metal nanostructures. Metasurface tweezers: Complex fabrication process involving nanostructures
Key technologies	Dual-fiber, single-fiber, and special-core fiber designs	Can be integrated with photonic chips and other devices, but may require more complex integration processes
Advantages	High flexibility, miniaturized design, suitable for complex environments	Nanoscale particle manipulation, high-precision sorting, and applications requiring strong field enhancements
Challenges	Limited by diffraction, lower capture forces for large particles	Plasmonic nanostructures, metasurfaces, and metaleenses
		Enhanced trapping capabilities, reduced laser power requirements, programmable particle trajectories
		Higher fabrication complexity, potential for photodamage due to high intensities

3.1.1 Single-cell precise manipulation

Since their invention in the 1980s by Arthur Ashkin [2], optical tweezers have found widespread application in biology, allowing precise control and measurement at the single cell level. One of the main application areas is the manipulation of individual cells for cell fusion, mechanical measurements, and sorting based on physical properties[115]. Optical tweezers exploit the radiation pressure exerted by a tightly focused laser beam to trap and manipulate dielectric particles, including cells, in three dimensions. A laser beam is focused by a high numerical aperture objective lens to create an optical trap. Particles near the focus experience a force due to the transfer of momentum from the scattering and gradient forces, which pulls the particle towards the center of the beam and traps it in place [116]. By steering the laser focus, the trapped particle can be moved with nanometer-level precision.

The application of optical tweezers to biological systems took off in the 1990s. In 1991, Block et al. used optical tweezers to study the movement of kinesin molecules along microtubules, demonstrating the technique's utility for precise measurements of molecular-scale forces and motion in biological systems [117]. Throughout the 1990s and 2000s, optical tweezers were increasingly applied to manipulate single cells and investigate cellular processes. For example, optical tweezers were used to study cell adhesion forces [118], measure the mechanical properties of cell membranes [119, 120], and even perform delicate intracellular surgery [121, 122]. One major application of optical tweezers is the study of single-cell mechanics[123–125]. By trapping and manipulating individual cells, researchers can measure their mechanical properties, such as stiffness and deformability, which play crucial roles in cell function and disease [126]. Sraj et al. used optical tweezers to study the deformability of red blood cells in patients with sickle cell disease, finding that these cells were stiffer and more susceptible to damage compared to healthy cells [127], as shown by Fig. 7a. Fraczkowska et al. employed optical tweezers to investigate the mechanical properties of breast cancer cells, demonstrating that cancer cells were more deformable than normal cells [128], as shown by Fig. 7b. Optical tweezers have also been used to study cell-cell interactions with high precision. Schmidt et al. investigated the cytoskeletal association and surface dynamics of β 1 integrins on the dorsal side of migrating fibrocytes using laser optical tweezers and nanoscale motion analysis [129]. Hashimoto et al. created cell assembly with the help of optical tweezers by using a polyethylene glycol (PEG) solution [130], as shown by Fig. 7c. They propose a theoretical model to describe the intermembrane stable energy due to depletion interaction and discuss the physicochemical mechanism of intercellular repulsion.

More recently, optical tweezers have been applied to high-throughput cell sorting based on intrinsic cellular properties. The optical tweezers technology adopted by Diao et al. in the AI-RACS system is a system that integrates the AI-assisted image recognition algorithm and optical tweezers technology, which is used to achieve accurate single-cell recognition and high-quality single-cell Raman spectrum acquisition [131], as shown by Fig. 7d. The system is coupled with optical tweezers technology to capture single cells through optical tweezers to achieve high-quality acquisition of Raman spectra. The optical tweezers module is one of the four core functional modules of the AI-RACS system. Together with the microfluidic chip, single-cell Raman spectrum acquisition module and single-cell collection module, the optical tweezers module achieves the goal of efficiently and accurately mining functional microbial cells from complex environmental samples. Through this integrated technology, the AI-RACS system is able to accurately identify, sequence, and collect single cells, transforming microbial single-cell research from a low-throughput manual operation to a high-throughput automated workflow. Optical tweezers have also been integrated with other technologies to expand their capabilities in single-cell studies. Chan et al. combined optical tweezers with Raman spectroscopy to study the biochemical composition of single cells while manipulating them [132].

Optical tweezers have matured into a versatile tool for contact-free, precision manipulation of single cells. They have enabled significant advances in understanding cell mechanics, adhesion, motility and sorting purely based on physical properties. With continued improvements in integrated photonics, faster image processing, and intelligent control, optical tweezers are poised to accelerate the development of label-free, single-cell assays and clinical cell sorting applications. While optical forces are well-suited for cell-scale manipulation, they face challenges in operating over large areas or with high throughput compared to techniques like acoustic, magnetic or microfluidic manipulation. Hybrid manipulation techniques combining optics with these modalities are an active area of research. Over the past decade, optical tweezers have continued to advance and find new applications in single-cell studies. From measuring cell mechanics and interactions to enabling high-throughput, label-free cell sorting, optical tweezers have proven to be a versatile and powerful tool for single-cell manipulation and analysis. As optical trapping technology continues to develop and integrate with other methods, it will likely play an increasingly important role in advancing our understanding of single-cell biology and its applications in biomedical research.

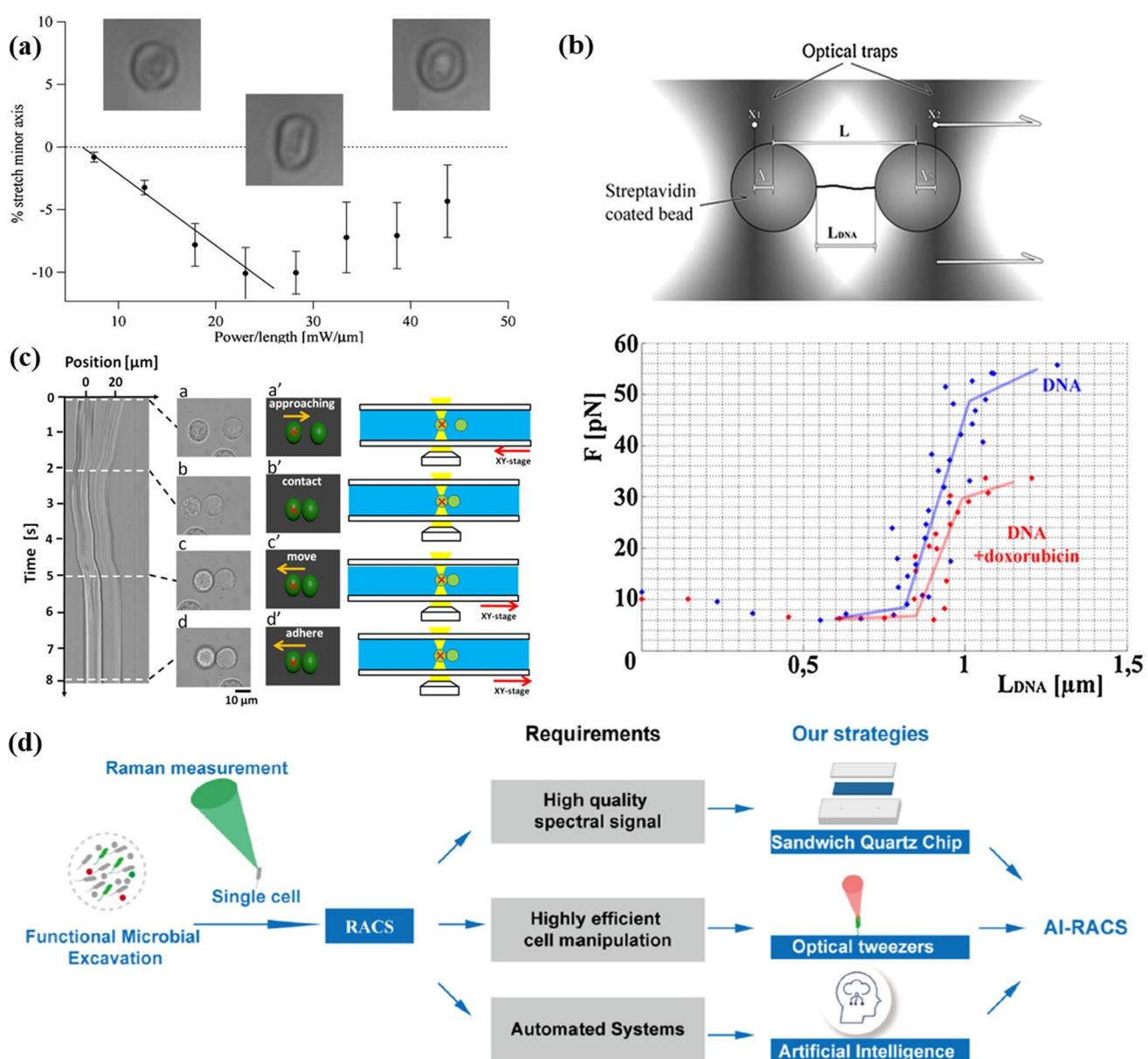


Fig. 7 **a** As the applied laser power increases, the subaxial stretch (%stretch) of the red blood cells also increases, and there is a clear linear relationship between the stretch and power in the low power region [127]. **b** The stretching process of two polystyrene beads connected by a single strand of DNA, and the force and molecular length properties of a DNA molecule with or without Adriamycin [128]. **c** The process of manipulating cells using laser tweezers in conditions containing 40 mg/ml PEG. Under this condition, cell-cell contact remains stable during transport [130]. **d** Strategies for developing automated and efficient artificial-intelligence-assisted automatic raman-activated cell sorting platforms [131]

3.1.2 Multi-cell parallel manipulation

The ability to precisely manipulate multiple biological cells simultaneously has tremendous potential for advancing our understanding of cellular interactions, tissue engineering, and regenerative medicine. Holographic optical tweezers (HOTs) have emerged as a powerful tool for non-contact, precise manipulation of microscopic objects such as cells. By dynamically shaping light through holography, HOTs can create multiple traps to control the 3D arrangement and interactions of cells. This has opened up exciting applications in tissue engineering, cell biology, and biophysics. The ability to manipulate many cells in parallel using HOTs has been transformative for studying multicellular systems. It enables the construction of artificial tissues with defined cellular organization, preparation of ordered cell arrays for high-throughput analysis, and probing of cell-cell interactions in well-controlled microenvironments.

HOTs utilize the optical gradient force to trap cells. A tightly focused laser beam creates a strong electric field gradient near the focus. Dielectric particles, like cells, are pulled to the point of highest intensity at the center of the focus. By modulating the phase or intensity of the light with a dynamic hologram, the optical trap can be split, translated, and customized. The hologram is usually generated by a spatial light modulator (SLM), a programmable diffractive optical element. Computer-generated holograms displayed on the SLM shape the phase and/or amplitude of the input laser beam. With appropriate algorithms, an arbitrary pattern of optical traps can be produced at the sample plane to simultaneously control the position of multiple cells. Trap stiffness, a measure of the applied force, scales with laser power. Trap geometry and resolution are governed by the objective lens numerical aperture and laser wavelength. Near-infrared lasers are typically used to minimize photodamage in biological samples. According to a historical review by Ashkin [133], the concept of optical tweezers was first demonstrated by Arthur Ashkin and colleagues at Bell Labs in 1986. They showed that a tightly focused laser beam could trap and manipulate microscopic objects, including living cells, through radiation pressure. This work built on Ashkin's earlier research into the effects of laser light on particles. In the early 1990s, several groups began exploring the use of optical tweezers for parallel manipulation of multiple objects simultaneously. Sasaki et al. [134] described the first use of computer-generated holograms to create multiple optical traps, allowing them to simultaneously manipulate over 10 microscopic particles. Dufresne and Grier [135] advanced this "holographic optical tweezer" (HOT) approach using diffractive optics to generate complex, dynamic trapping patterns. A key breakthrough for multicellular manipulation came from Grier's lab with the development of a real-time HOT system incorporating adaptive optics [136]. This enabled the 3D positioning and orientation of trapped objects to be dynamically updated at video rates. The authors applied the system to manipulate yeast cells and other microorganisms, highlighting its potential for biophysical research. Subsequent work extended HOT-based multicellular manipulation to a variety of biological systems. Akselrod et al. [137] used the approach to precisely arrange bacterial and yeast cells into ordered 2D structures to study intercellular interactions.

HOTs have found increasingly sophisticated applications in cell manipulation, tissue engineering, and biophysics. For instance, HOTs have been used to assemble multiple cell types into precisely-controlled 3D architectures mimicking natural tissues. Kirkham et al. used HOTs to print 3D networks of stem cell spheroids and directed their differentiation [138], as shown by Fig. 8a. The same group further demonstrated the precision assembly of complex cellular microenvironments using HOTs. Moreover, HOTs allow precise control over the contacts between cells to study how mechanical forces and interactions influence cellular behavior. Bambardekar et al. used HOTs to study the role of cell-cell adhesion in the formation of 3D cellular aggregates [139], as shown by Fig. 8b. Muhamed et al. investigated the mechano transduction of cell-cell junctions using HOTs combined with microfluidics [140]. Furthermore, HOTs have been widely used for the manipulation and analysis of individual cells. Zhang and Liu reviewed the applications of optical tweezers in single-cell studies, including cell sorting, cell-cell interaction analysis, and cell mechanics measurements [12]. Agarwal et al. used OTs for automated cell sorting based on fluorescence signals [141]. Correspondingly, the ability of HOTs to apply precise forces to multiple cells simultaneously enables the study of cellular biomechanics. Yousafzai et al. used HOTs to measure the viscoelastic properties of individual cells [142], as shown by Fig. 8c. Tan et al. probed the mechanics of cell–matrix interactions using HOTs [143].

In summary, the development of HOTs has enabled increasingly flexible and precise parallel manipulation of living cells and multicellular structures. Over the past few decades, the technique has matured into a powerful tool for basic biological research and biomedical applications. Continued advances seem likely to further extend its capabilities and impact. The key advantages of HOTs include parallel manipulation of multiple cells with independent control, assembly of complex 3D multicellular structures, precise force measurements for studying cellular biomechanics. However, HOTs also have some limitations. Future development of HOTs will likely focus on improving system throughput, integrating real-time image processing and force feedback [144], and extending manipulation capabilities in 3D [145]. Combining HOTs with microfluidics [140] and machine learning [146] will enable intelligent, automated cell handling for high-throughput applications. Advances in SLM technology and computational methods will expand the applications of HOTs in cell biology, tissue engineering, and regenerative medicine [43, 147].

3.2 Manipulating artificial microstructures

Through such as metasurfaces and metalenses, multi-dimensional manipulation of the light field can be realized, and then particles can be controlled by manipulating the light field. In recent years, there have been optical manipulation by utilizing imaginary poynting momentum [148, 149]. However, the light field itself also has a mechanical effect on the object it illuminates, and this effect can be controlled by cleverly designing the microstructure being irradiated,

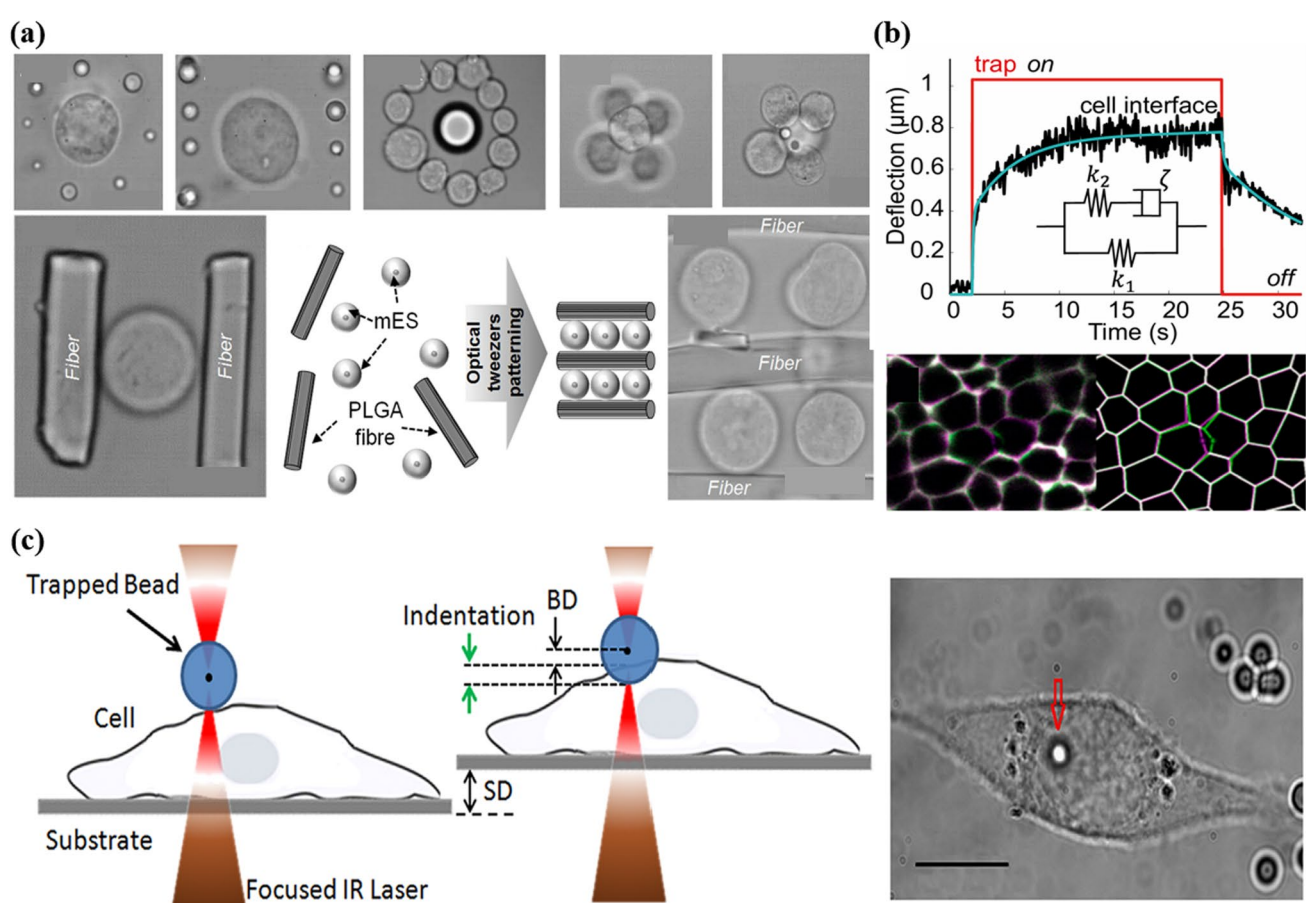


Fig. 8 **a** The ability to precisely manipulate mouse embryonic stem cells (mES) and poly(lactic-glycolic acid) copolymer (PLGA) particles and electrospun fibers to form predetermined structures was demonstrated using HOTs technology [138]. **b** The shift of the cell–cell interface during trap on and trap off laser tweezers. The superimposed diagrams of the undeformed (purple) and deformed (green) tissues in the experiment are shown on the left, and the corresponding superimposed diagrams of the simulated tissues are shown on the right [139]. **c** The processes of cell localization and interaction between cells and microbeads are described. Microbeads are captured by optical tweezers and used to study the mechanical properties of cells. With this setup, the researchers were able to control the interactions between the cells and the microbeads and measure the resulting forces and displacements, which in turn calculated the elastic modulus of the cells [142]

creating a micromanipulation effect that is completely different from that of optical tools such as optical tweezer or optical spanner[150], and is not subject to the characteristics of the incident light field [24, 151]. In this section, we will review the latest progress in the field of optical field-driven artificial microstructures in recent years, and prove its important role and great potential in the field of optical micromanipulation, paving the way for the development of optical micromanipulation in the future.

3.2.1 Light-driven micromotors

Traditional dielectric particles or metal particles have a relatively simple response to the external light field, and complex optical manipulation cannot be achieved through a simple incident light field. By carefully designing the shape and size of the particles, or using a special arrangement of multiple particles, it can form a local strong electric field or asymmetric dipole when the light field is incident, so that it produces strong one-way scattering, and then produces great optical force. Based on this characteristic, researchers can manipulate the scattering direction of light to achieve complex manipulation of particles. In addition, because the particle itself is small and has the characteristic of responding independently to the light field, it can be embedded in the micro-nano media block to make it perform a function similar to that of a "drone motor" under the irradiation of the external light field. A simpler artificial micromotor is a gear-like structure composed of multiple gold blades. In 2010, Liu et al. used four equal arms of L-shaped gold leaves to form an artificial micromotor with a horizontal "four-leaf clover" structure, and realized the two-way rotation of the micromotor

under conventional linearly polarized light incidence, and the rotational moment of the bidirectional drive reached a significant peak at 810 nm and 1700 nm incidence, respectively, as shown in Fig. 9a [152]. The micromotor is embedded in the silicon nano-disk, and the light torque it receives can drive the silicon nano-disk with an area of 4000 times its body to rotate, and the driving effect will be further enhanced by increasing the number of motors. The light moment of the structure is only related to the symmetry of its own structure and its interaction with the incident light, and the incident of linearly polarized light causes it to symmetrically produce the non-uniform distribution of the local electric field on the four blades, and then produces a momentum flow in the off-center position, and the overall performance is to produce the optical moment of the micromotor. Fourteen years later, Hong et al. designed a metal nano-kirigami micromotor with a spur gear structure on the outer ring and an upward-turned spiral blade structure on the inner ring, as shown in Fig. 9b. It can shift from a horizontal state to a vertical state for in-situ rotation and pure rolling in the irradiated area [153]. This feature allows the micromotor to operate the micro-slit to switch on and off and to traverse the micro-slit with complex shapes. The strong optical force on the micromotor, causing it to tumble from a flat state to a vertical state. In the vertical state, when the micromotor deviates from the center of the irradiation area, an asymmetrical electrophoresis force is applied to the gear of the outer ring to make it roll towards the center, and the pure rolling of the micromotor can be achieved by moving the photoelectric tweezers irradiation area.

At the same time, the asymmetry of the structure can also be used to produce directional scattering of the light field. In 2017, Tanaka et al. used triangular metal particles to achieve one-way scattering towards one sharp corner of the triangle, or simultaneous one-way scattering in two sharp directions [158]. Three years later, they ingeniously designed an artificial micromotor consisting of two gold nanorods of different lengths placed in parallel, such as Fig. 9c [154]. Unidirectional scattering under plane wave irradiation is achieved and a transverse recoil optical force is provided, the direction of which is independent of the incident light and is determined only by the direction of the nanorods. In addition, by embedding multiple micromotors into the silica micro-blocks in a special arrangement, the linear drive and rotation of the whole particle under plane wave irradiation are realized, and the driving speed is proportional to the irradiated light intensity. The structure takes advantage of the strong and highly directional scattering allowed by nanoparticles with dipole plasma resonance at different frequencies, so that the micromotor generates a pair of detuned dipoles under illumination, which excites one-way scattering perpendicular to the direction of the nanorods, thereby producing a recoil transverse light

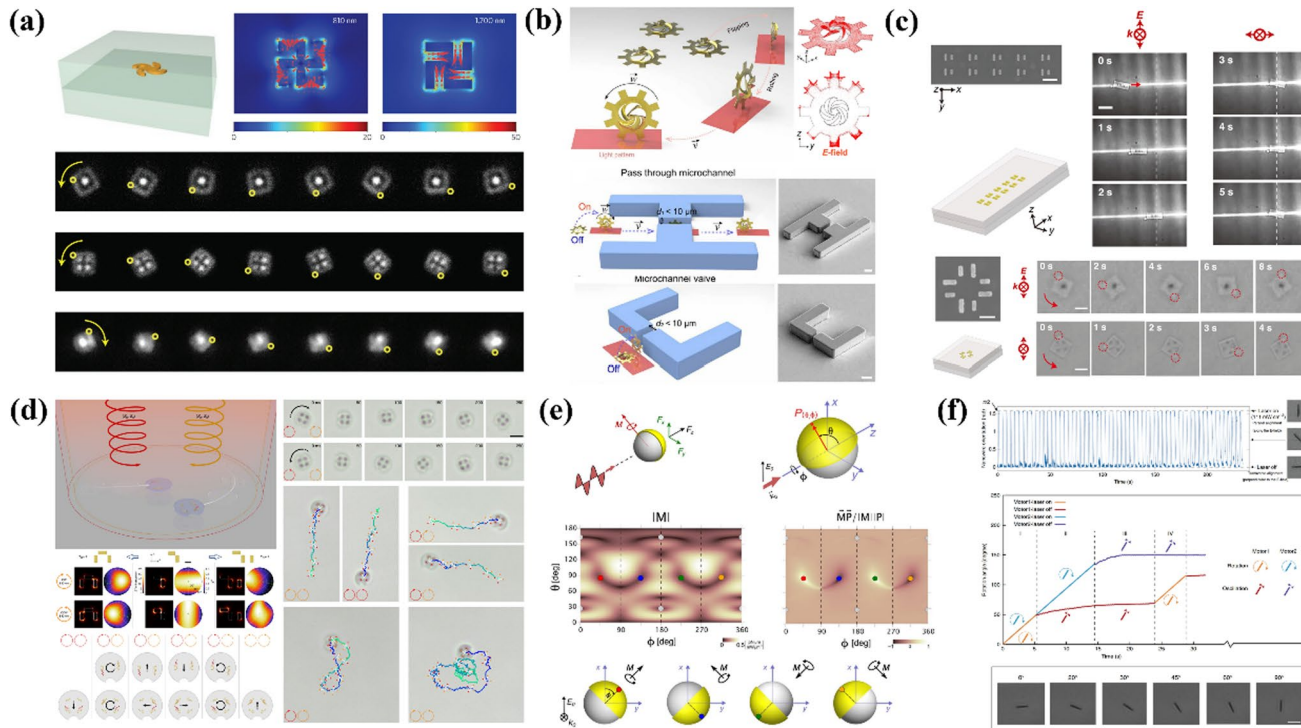


Fig. 9 Light-driven micromotors. **a** Surface plasmonic micromotors[152]. **b** Nano-kirigami micromotor[153]. **c** Transverse optical forces induced by detuned dipoles[154]. **d** Two-dimensional free light-driven micro-nano drones[155]. **e** Janus particle micromotors with spin steady[156]. **f** Semiconductor nanowires with fast switchable alignment[157]

force on the whole structure. Inspired by the above work, in 2022, Wu et al. designed an artificial micromotor composed of three gold nanorods vertically, and by embedding them into the nano disk to form a "micro-nano drone", it realized the free motion of the whole in the two-dimensional plane under the irradiation of two circularly polarized lights with different chirality and wavelengths of 930 nm and 980 nm, respectively, such as Fig. 9d [155]. The irradiation of the Au-nanorod array by circularly polarized light will cause a local induced electric field enhancement on the surface of the A-nanorods, which is asymmetrical, so that the overall structure interacts with the incident light field, and produces an asymmetrical directional optical force on the structure itself. The combination of multiple such arrays can generate optical forces and optical moments in any direction, so as to realize the two-dimensional free control of micro-nano drones.

In addition, some specially designed structures or dielectric particles can form a spin or alignment steady state under the irradiation of an external light field, which can also play the function of a micromotor. As an example, in 2017, Ilic et al. designed a gold-plated Janus particle with a hemispherical surface of silicon nanospheres, which can be transformed into a stable nanoscale micromotor under specific spectral irradiation, such as Fig. 9e [156]. The stable spin state of multiple orientations of the particle under the incident of a plane wave is realized. At the same time, it was proved that in the absence of external optical angular momentum, spin particles can still be formed. The interaction between the plane wave light field and the dielectric nucleus-metal-coated Janus particles can form phase space, in which the topological protection anti-cross behavior of the vortex of the torque vector field leads to the emergence of spin steady. Subsequently, in 2019, Liang et al. found that semiconductor nanowires can be quickly aligned under visible light irradiation, and realize their rapid switching of parallel and perpendicular directions of the incident electric field, making them have the function of artificial micromotors, such as Fig. 9f [157]. Visible light alters the imaginary part of the electric field of semiconductor nanowires, which can be reflected in drastic changes in the direction and speed of rotation in a high-frequency rotating electric field. The imaginary part and the real part of the electric field are related by the Kramers–Kronig relation, so that when the imaginary part of the electric field is changed by external stimuli, the real part of the electric field will also change at the same time. By using the interaction of the artificial micromotor with the light field, a strong local electric field can be generated and the scattering direction of the light can be controlled, or a steady state can be formed, and then the motion of the entire micro-nano particle including the micromotor can be manipulated. This not only demonstrates the diversity and extraordinary potential of micro-optics in driving and controlling the motion of objects, but also paves a new path for the research and development of light-driven micro-nano robots in the future.

3.2.2 Light-driven micro-machinery

In the field of optical micromanipulation of micro-nano robots, parallel to micromotors is the rise of a series of artificial micro-nano machines. Different from embedding multiple independently controllable artificial micromotors into the dielectric micro-block to realize the optical drive of the micro-nano robot, the artificial micro-nano machine usually combines the entire metasurface with the substrate, and uses the complex response of the metasurface to the light field, which in turn acts on the micro-nano machine itself to achieve complex optical micro-manipulation. In 2021, Andrén et al. fabricated a optical grating metasurface (OGM) arranged by arranging square nano-silicon nanocolumns by processing silicon-based micro-nanostructures on insulators [159]. The micro-nano machinery was released into water, and the sample was irradiated with 1064 nm lasers of linear polarization and circular polarization, respectively, and the unidirectional scattering of the incident light by OGM generated a recoil lateral optical force (LOF), and then the unidirectional drive under linear polarization and the circumferential trajectory drive under circular polarization were realized, such as Fig. 10a. Because they experimentally achieved an artificial micro-nano machine driven by a non-tightly focused light field for the first time, they named it "Meta-vehicle". Subsequently, in 2022, by combining with geometric phase metasurfaces (GPMs), Qin et al. adjusted the spacing of nanopillars on metasurfaces to generate Fano resonances, and then fine-tuned the structural parameters of their unit structures to change the position of the formants, realizing a bound state in the continuum (BIC) based metavehicle, as shown in Fig. 10b [160]. However, both of these micro-nano machines lack the degree of freedom to adjust the polarization direction of the scattered light, so they can only achieve one-way drive, and they lack a "reverse" function compared to the cars that people drive in their daily lives. Therefore, based on the idea of perfecting a full-featured supercar, in early 2023, Li et al. designed and reported a supercar combined with a specially designed phase gradient metasurface (PGM) [161]. On the basis of the work of its predecessors, it realizes the two-dimensional full-freedom handling of super-structured sports cars, such as Fig. 10c. By changing the linear polarization angle of the incident light, the PGM will switch the scattering direction of

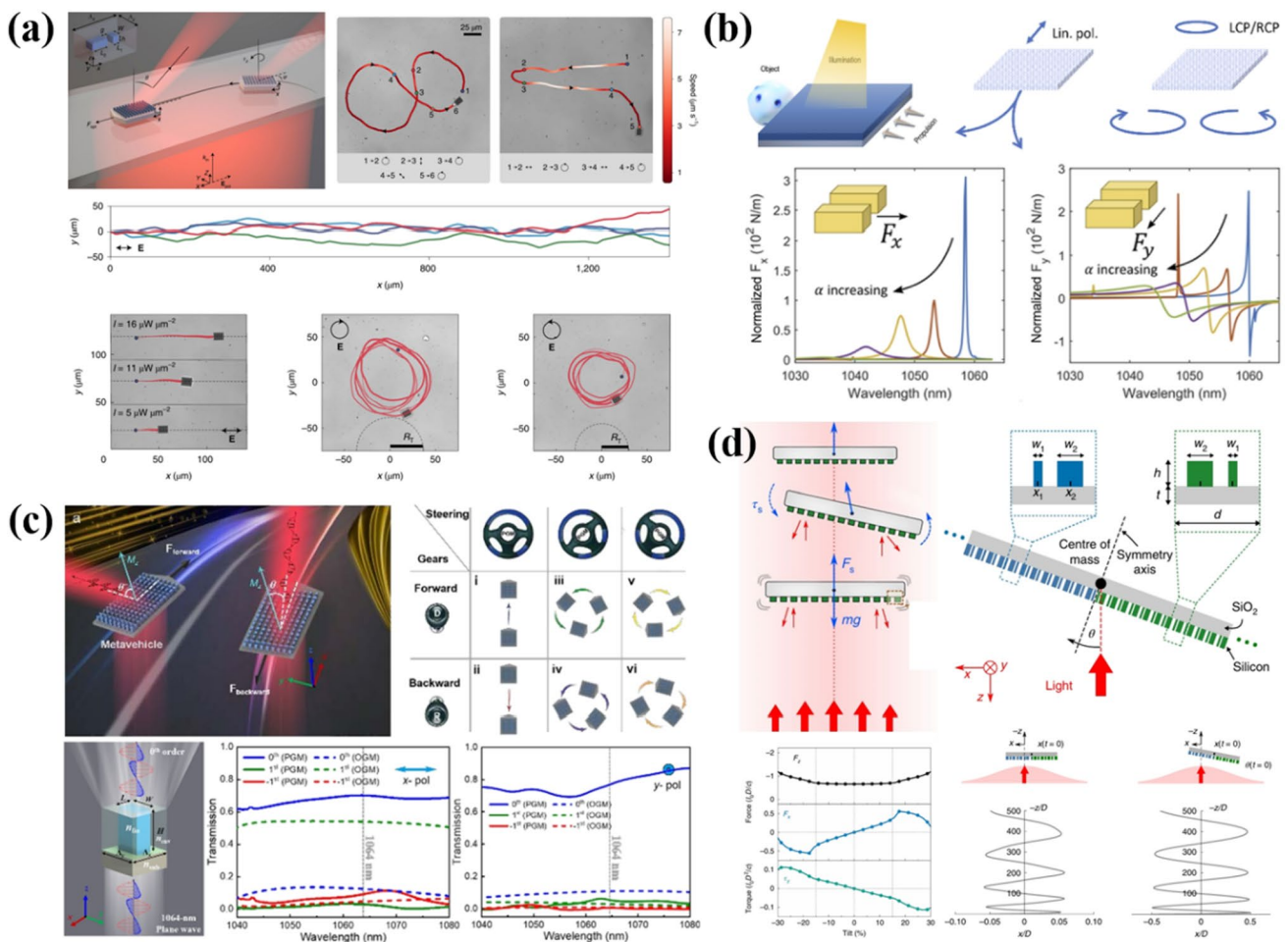


Fig. 10 Light-driven micro-machinery. **a** OGM-based metavehicle and its experimental results[159]. **b** BIC-based metavehicle[160]. **c** A full-controlled PGM-based metavehicle [161]. **d** Self-stabilizing optical suspension of dielectric metasurface in vacuum [163]

the scattered light, so as to realize the direction switching of the recoil LOF, so that the supercar has an additional "reversing" function on the original basis. This design not only fully realizes all the movements of the supercar in the two-dimensional plane: forward, backward, turn left and turn right, but operates more efficiently due to the device's zero diffraction order. In addition to metavehicle, more recently, Engay et al. have proposed a metaspinner combined with metagrating[162]. It is driven by a transverse optical gradient force, which can realize the reverse rotation manipulation of spin and revolution, and broadens the degree of freedom of manipulation of light-driven micromachinery.

The application of micro-nano machinery is far from being limited to this. In addition to the liquid environment, it also has an extraordinary performance in the vacuum environment. In 2019, Ilic et al. used the special periodic arrangement of asymmetric silicon nanopillars to design a micro-nano machine called "metasurface elements for passive stabilization (MEPS)", such as Fig. 10d [163], whose asymmetrical cell structure produces an asymmetrical scattering response. Therefore, when the micro/nano machinery is tilted or offset relative to the laser beam, a recovering optical moment is generated, prompting it to return to its original equilibrium position. This makes it possible to achieve self-stabilizing manipulation of objects in the laser beam. In addition, the combination of multiple MEPS enables stable optical manipulation of objects with multiple degrees of freedom. The study of micro-nano mechanics has shown us a new possibility of metasurfaces, which can also be manipulated by light fields as objects themselves, which opens a new door in the field of optical micromanipulation.

4 Interdisciplinary nano-optic manipulation

4.1 Photonic chips

Optical tweezers and manipulation techniques have emerged as powerful tools for precisely controlling and manipulating cells and other microscopic particles. Traditionally, these systems have utilized ordinary optical fibers to deliver the trapping laser beam. However, the advent of photonic integrated circuits and chips has opened up new possibilities for miniaturizing and enhancing the capabilities of optical manipulation[164].

Photonic chips integrate waveguides, couplers, interferometers, and other optical components onto a compact substrate, enabling complex light routing and shaping on a microscale. When applied to optical tweezers, photonic chips allow the generation of sophisticated optical trapping geometries beyond what is possible with single optical fibers. The working principle of photonic chips for optical trapping involves harnessing the synergistic effects of the gradient force and scattering force induced by the interaction of the structured light field with the trapped particle. The gradient force arises from the spatial gradient of the light intensity and acts to pull particles towards the region of highest intensity. This is the force primarily responsible for stable trapping in conventional optical tweezers. On the other hand, the scattering force is a result of photons scattering off the particle and imparting momentum, which can push particles along the beam propagation direction. By carefully designing the photonic circuit and optical mode profile, the balance and interplay between the gradient and scattering forces can be optimized for efficient trapping and manipulation.

Photonic chip-based optical tweezers offer several advantages over traditional fiber-based systems. The ability to generate complex light patterns and trapping arrays on-chip allows for the parallel manipulation of multiple cells or particles. The miniaturization enabled by photonic integration also makes these systems more compact, stable, and power-efficient. Furthermore, the planar geometry of photonic chips facilitates the integration of microfluidic channels for sample delivery and sorting, enabling seamless on-chip manipulation and analysis. This section aims to provide a comprehensive overview of the current state-of-the-art in photonic chip-based optical tweezers and manipulation techniques.

4.1.1 Manipulation based on light gradient forces

Optical gradient forces arise when a particle, such as a waveguide, experiences a force in the direction of increasing optical intensity. By engineering structures like waveguides, resonators, and photonic crystal cavities to shape the optical intensity profile, these forces can be harnessed for functions like optical switching, modulation, and sensing on photonic chips.

The working principle behind optical gradient force-based photonic chips is the interaction between light and matter at the nanoscale. When light is confined to sub-wavelength structures like photonic waveguides or cavities, strong intensity gradients are generated. Dielectric particles near these gradients experience an attractive force towards regions of high optical intensity[147]. The strength of the optical gradient force depends on the particle's polarizability and the intensity gradient. For waveguides, the evanescent field extending from the waveguide core creates an intensity gradient and attractive force on nearby particles. In cavities and resonators, light is trapped in a small volume, generating large field gradients.

Optical waveguide couplers enable efficient light transfer between adjacent waveguides. Wiederhecker et al. [165] demonstrated that by introducing a nonuniform gap between coupled waveguides, an attractive optical force can be generated, leading to improved light coupling from one waveguide to another. This concept of gradient force-based coupling has been further explored by Apiratikul et al. [166], who investigated the nonlinearities in GaAs microdisk resonators. While their study primarily focused on resonators, the principles of nonlinear optical interactions and the role of optical forces in coupling are relevant to the design and optimization of waveguide couplers.

Optical resonators enable various functionalities such as wavelength filtering, optical delay, and nonlinear optical interactions. Researchers have explored the use of optical gradient forces to improve the performance of these resonators. Li et al. [167] proposed a gradient force-based resonator design that employs a looped waveguide geometry with a narrowed coupling region, resembling a racetrack configuration. This design leverages the attractive optical force in the coupling region to enhance light confinement and mitigate losses. Wiederhecker et al. [168]

further investigated this concept and demonstrated broadband tuning of optomechanical cavities using optical gradient forces. Their work highlights the potential of gradient force-based resonators for applications requiring tunable and high-performance optical cavities.

Gradient force-based photonic chips have seen significant progress and diversification in recent years. Researchers have pushed the capabilities of these devices to new levels of performance, efficiency, and application.

In 2010, Gong et al. demonstrated a silicon photonic crystal cavity with a quality factor exceeding one million, enabled by gradient force optimization [169]. The high-Q cavity paved the way for enhanced light-matter interactions and nonlinear optics on chip. Zhang et al. developed a gradient force-based nanomechanical waveguide coupler in 2012 [170]. The device utilized an optomechanical interaction between a suspended silicon nitride waveguide and a nanobeam, achieving tunable coupling with a bandwidth of 500 kHz. In 2015, Phare et al. realized a gradient force-actuated graphene electro-optic modulator [171]. The modulator employed a graphene-silicon hybrid waveguide with an asymmetric cross-section, enabling efficient modulation with a voltage-length product of 0.2 V·μm. Otterstrom et al. demonstrated a gradient force-enhanced Brillouin laser in 2018 [172]. The laser coupled a silicon nitride waveguide with an acoustic resonator via gradient forces, achieving a threshold of 5 mW and a linewidth of 100 Hz. In 2020, Bogaerts et al. developed a programmable photonic processor based on gradient force-actuated phase shifters [173]. The processor employed a mesh of Mach-Zehnder interferometers with tunable couplers, enabling arbitrary linear transformations with a reconfiguration time of 10 μs.

Applying machine learning techniques, Gong et al. designed a gradient force-based photonic neural network in 2019 [174], as shown by Fig. 11a. The chip featured an array of racetrack microresonators interconnected by controllable waveguide couplers, emulating the synapses and neurons in the brain. The device performed learning tasks such as vowel recognition with low latency and energy consumption, highlighting the potential of gradient force photonics for neuromorphic computing.

Expanding the application scope, Marchetti et al. realized a gradient force-actuated photonic lab-on-a-chip in 2021 [175]. Micro-patterned waveguide surfaces generated strong near-field gradient forces to trap, manipulate and sense biological specimens like cells and nanoparticles. The planar photonic interface offered a versatile platform for compact and scalable bio-photonic analysis.

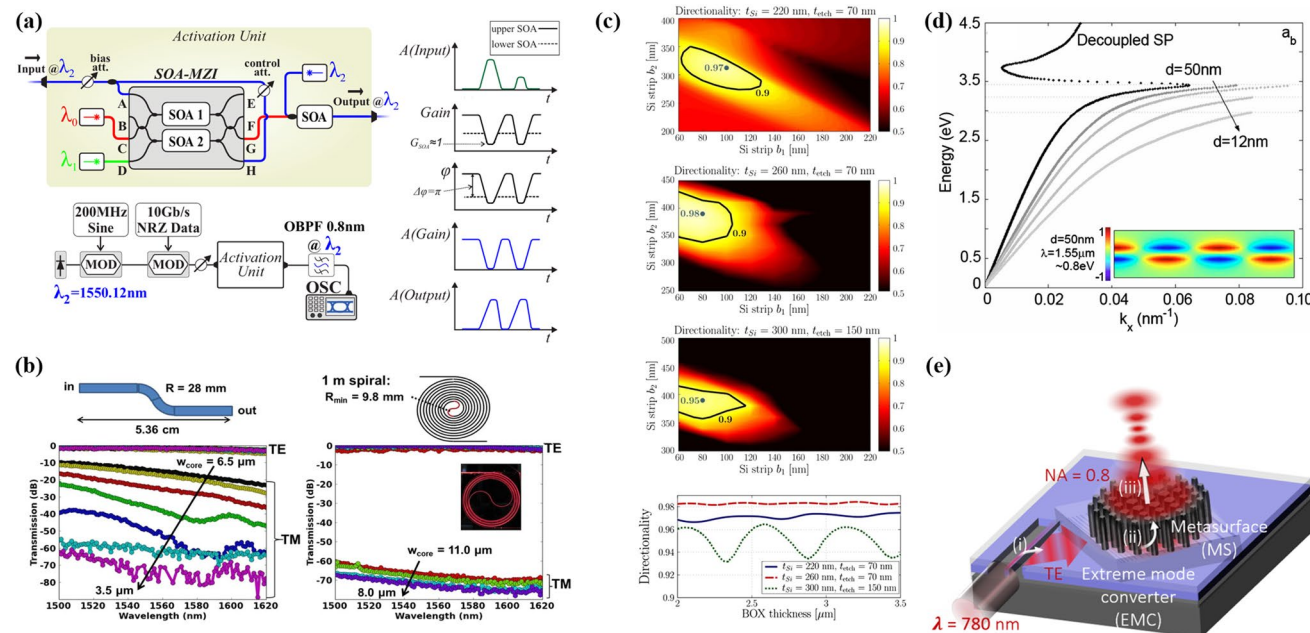


Fig. 11 **a** The operating principle of the all-optical threshold, including the control pulse injection, gain response, phase response and the change of the output signal, and the experimental setup diagram for measuring the characteristics of the transfer function [174]. **b** Transmission characteristics of S-bend and helical waveguide with different core widths [175]. **c** The influence of strip width (b1 and b2) on grating directivity in grating coupler design with different silicon layer thickness (tSi) and different etching depth (tEtch). The grating directivity changes with the thickness of BOX (Buried Oxide) layer under different grating geometry [176]. **d** Antisymmetric Field model dispersion relation and electric field distribution [177]. **e** The photon waveguide mode is converted into a free-space beam in three stages, and the beam is precisely shaped and focused using metasurface [178]

Gradient force-based photonic chips offer unique advantages such as strong light confinement, low-power actuation, and compatibility with CMOS fabrication [180]. However, challenges remain in the precise control and scalability of gradient force structures. Future research directions include the integration of gradient force devices with active photonic components, the development of large-scale neuromorphic photonic systems, and the exploration of quantum photonic applications [181]. With ongoing advances, gradient force-based photonic chips hold promise for enabling new paradigms in optical information processing, sensing, and communication.

4.1.2 Manipulation based on light scattering forces

When light is reflected, refracted, or scattered by a material, there is an associated transfer of momentum that generates optical forces [1]. These forces are extremely small at the scale of everyday objects. However, at the microscopic scale relevant to photonic chips, they can be harnessed to physically manipulate light. The nature and magnitude of the optical force depends on the intensity, wavelength, and polarization of the light as well as the optical properties of the material it interacts with. Importantly, by structuring a material to have spatially-varying optical properties, the optical forces can be tailored to guide light along desired paths [182].

Early research on photonic chips based on light scattering forces focused on demonstrating basic light guiding and manipulation functionalities. In 2004, Vlasov et al. demonstrated a silicon waveguide that could guide light with low loss over centimeter-scale distances on a chip [183]. In 2006, Vlasov et al. showed that light could be slowed down and stored in a photonic crystal waveguide using light scattering forces [184]. These preliminary results laid the foundation for more advanced photonic chip structures.

Some of the key photonic building blocks that enable light manipulation on a chip using scattering forces include straight dielectric waveguides, surface plasmon waveguides, grating couplers and so on.

Straight dielectric waveguides are the simplest structures, consisting of a high refractive index material surrounded by lower index cladding. Light is guided by total internal reflection. Scattering forces arise at the core-cladding interfaces. Simple straight waveguides were the first structures used to guide light on photonic chips. They have been optimized for low loss and high confinement using techniques such as shallow ridge waveguides and slot waveguides [185].

Surface plasmon waveguides consist of a metal film adjacent to a dielectric. Surface plasmons can confine light to sub-wavelength dimensions but suffer from higher losses compared to dielectric waveguides. Scattering forces arise from the momentum transfer associated with plasmon propagation. In 2006, researchers demonstrated a surface plasmon waveguide on a photonic chip that could guide light with low loss over 100 μm distances [186].

Grating couplers are periodic structures that can couple light from a free-space beam into a waveguide and vice versa. They are essential for getting light on and off a photonic chip. Periodic structures cause light to diffract at specific angles depending on the spacing. By varying the grating period, light can be directed in or out of plane. The associated momentum changes generate scattering forces. In 2002, Taillaert et al. demonstrated efficient grating couplers with over 30% coupling efficiency [187].

By combining these and other building blocks, complex photonic circuits can be created to route and process optical signals on a chip. Just in the past few years, several major advances have been made demonstrating the increasing maturity and potential of this technology.

In 2013, Bauters et al. demonstrated a silicon waveguide with a record-low propagation loss of 0.1 dB/cm, enabled by a new fabrication process that minimizes sidewall roughness [175], as shown by Fig. 8b. In 2016, Li et al. demonstrated a surface plasmon waveguide coupled to a high-quality factor microcavity, paving the way for ultra-compact, low-power optical switches and sensors [188]. In 2015, researchers designed a silicon-based fiber-chip grating coupler that combines interleaved trenches and a subwavelength index-matching structure to achieve high directionality and low coupling loss [176], as shown by Fig. 8c. The fabricated grating coupler demonstrates a measured coupling efficiency of -1.3 dB , a 3 dB bandwidth of 52 nm. The proposed grating coupler design offers a practical solution for efficient and robust fiber-chip coupling in silicon photonic integrated circuits.

Using scattering forces for on-chip light manipulation offers several advantages, including enabling all-optical control, allowing components to be extremely compact and integrable in large-scale silicon photonics, providing a large design space for a wide variety of effects and geometries.

However, there are also some notable challenges. First, pushing the limits of waveguide loss and confinement. New materials and fabrication techniques to enable lower loss and tighter light confinement will continue to be a major focus. Integrating atomic-scale materials like graphene with photonic chips is a promising direction [189]. Second, expanding the applications of surface plasmon devices. While challenging, the unique capabilities of surface plasmons for sensing

and nonlinear optics will drive further research into integrating them with practical photonic chips. New designs to minimize loss and improve coupling efficiency will be critical [190]. Third, increasing the efficiency and bandwidth of grating couplers. More efficient and broader-bandwidth grating coupler designs will be essential as photonic chips scale to higher levels of complexity and functionality. Inverse design and topological optimization techniques show promise for pushing grating coupler performance [191]. Last, system-level integration. A key challenge will be integrating these various photonic building blocks together into full systems that can solve real-world problems in communication, computing, and sensing. Co-packaging photonics with electronics and developing new architectures that leverage the unique properties of light will be important [192].

With ongoing advances, scattering-force photonics has the potential to enable ultra-fast, low-power technologies for communications, sensing, and computation.

4.1.3 Combined application of gradient and scattering forces

Optical manipulation in photonic chips relies on two key forces: the optical gradient force and the scattering force. The optical gradient force arises from the interaction between light and the refractive index gradient in a material, which can attract or repel particles towards regions of high or low light intensity. The scattering force, on the other hand, is caused by the transfer of momentum from photons to particles, resulting in a pushing effect along the direction of light propagation. By carefully designing the photonic structures, such as waveguide arrays, multimode interference couplers, and ring resonators, researchers can harness these forces to control the flow of light on a chip [193]. For example, the optical gradient force can be used to trap and guide light in a waveguide, while the scattering force can be employed to switch or route light between different waveguides [177], as shown by Fig. 8d.

In 2007, Solmaz et al. reported the use of multimode interference couplers for optical sorting and switching of particles [194]. In 2018, Li et al. developed a ring resonator-based optical switch that could route light between two waveguides using the scattering force [195]. The device exhibited low insertion loss, high extinction ratio, and fast switching speeds, making it promising for optical communication systems.

A notable development is the integration of optical manipulation with other photonic functionalities on a single chip. In 2019, Yulaev et al. demonstrated a compact metasurface integrated photon platform capable of generating the desired free-space radiation field profile on the chip surface, including precisely controlled light focusing, polarization, and lateral intensity distribution [178], as shown by Fig. 8e. The device structure is based on three successive stages of waveguide to free-space mode conversion, including coupling using spatial variations, raster projection, and metasurface treatment. This multi-functional integration represents a significant step towards realizing complete lab-on-a-chip systems based on optical manipulation.

Looking ahead, photonic chips based on optical manipulation hold great promise for a wide range of applications, including optical computing, sensing, and communication. One key challenge is to further improve the efficiency and scalability of these devices. Another important direction is to explore the integration of optical manipulation with other emerging technologies, such as quantum photonics and neuromorphic computing. For example, optically controlled photonic circuits could be used to implement quantum gates and circuits [196], or to emulate the synaptic plasticity and learning capabilities of biological neural networks [197].

In conclusion, photonic chips based on optical manipulation have made significant progress over the past two decades, with various structures and applications being demonstrated. While challenges remain, the unique capabilities of optical gradient and scattering forces in controlling light on a chip hold great potential for enabling new paradigms in optical information processing. As research in this field continues to advance, we can expect to see more breakthroughs and innovations in the years to come.

4.2 Optofluidic and its applications

Optofluidic technology refers to the use of light to guide the flow of microfluidics and the movement of particles, so as to achieve integrated control of particle and fluid motion on the micron scale. The field has recently made tremendous progress thanks to the joint efforts of researchers from various scientific disciplines [198–202]. Combining optical tweezers with optofluidic technology can significantly improve the performance and efficiency of optical tweezers. At the same time, optofluidic technology has also achieved a series of extraordinary results in biomedical science. In this section, we will review the recent advances in the combination of optofluidic and optical tweezers in recent years and their latest applications in biomedical science.

4.2.1 Optofluidic tweezers

In recent years, with the development of optical tweezer technology, there are certain limitations in several aspects, such as only one or several particles can be manipulated at the same time, the control efficiency is low, and the specific particles in the solution cannot be accurately manipulated. Therefore, by combining it with novel optofluidic technology, a technique called " optofluidic tweezers" was created to overcome the limitations of optical tweezers. In recent years, significant progress has been made in combining optical tweezers with microfluidics, which has made it more widely used in multi-particle manipulation, particle screening [203], and accurate capture of individual particles in fluids [136, 204].

By utilizing HOT, it can achieve multi-particles manipulation [205], and in turns of combining holographic optical tweezers, it is possible to achieve more precise micromanipulation and monitoring of microfluidic channels. In 2019, Gao et al. proposed a dynamic holographic optical tweezer such as Fig. 12a. It is capable of manipulating a single micron-scale anisotropic particle in a microfluidic environment with the precision and stability required for X-ray Bragg diffraction experiments, allowing it to function as an "optical goniometer" [147]. At the same time, the method can also be extended to various X-ray related experiments. In addition, with the use of brighter coherent X-ray sources, the Bragg coherent diffraction imaging of individual particles in solution will also be significantly enhanced. In the same year, Lasnoy et al. proposed a new method for continuously controlled colloidal polymerization of polydimethylsiloxane based on optical traps induced by light traps in fluids in microfluidic channels, as shown in Fig. 12b [206]. When the fluid resistance on the polymerized colloids in the optical trap exceeds the light capture force, it leaves the optical trap and begins to polymerize the new colloids at the same location. Moreover, they demonstrated the reproducibility of the process and achieved the selective production of colloidal particles with a radius of about 1–14 μm by controlling the intensity of the incident laser and the flow rate of the microfluidics. In addition, the use of holographic optical tweezers can monitor the influence of multiple optical traps on the cross-section of microfluidic channels, thus forming a optical controlled assembly line for colloidal particle aggregation. By combining on-chip waveguide optical tweezers, high-efficiency capture of particles can be achieved. In 2022, Walker et al. demonstrated an optofluidic device like Fig. 12c shows that it uses optical scattering forces and optical gradient forces to trap particles in microchannels with a thick film of 300 nm [207]. On-chip waveguides are used to direct incident light into the microfluidic capture channel. The light scattering force is used to push particles into the protruding cavity at the edge of the channel, isolating the particles from the microfluidics within the main channel, thus achieving the capture of the particles. At the same time, they also proposed two microfluidic devices, which use only the scattering force and the scattering force and gradient force, respectively, with the former having a capture

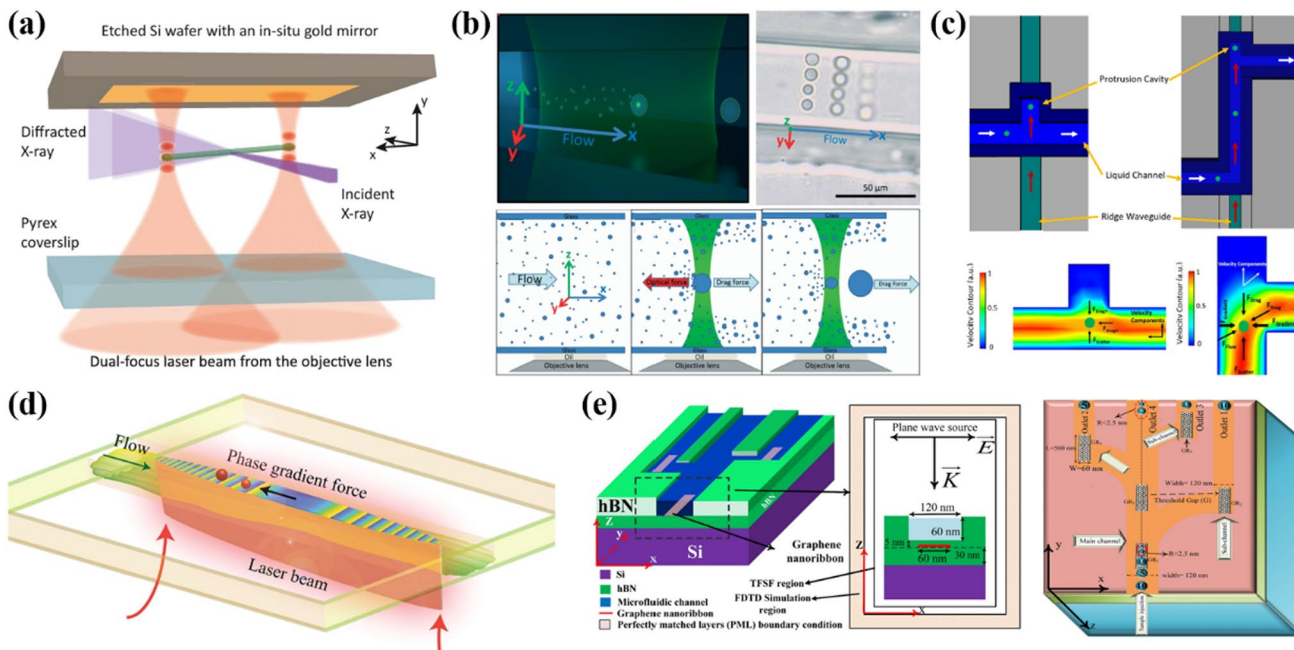


Fig. 12 Optofluidic tweezers. **a** Capture and align particles using a bifocal standing wave optical trap [147]. **b** Optofluidic holographic tweezers drive colloidal particle polymerization [206]. **c** On-chip waveguide-based optofluidic tweezers [207]. **d** On-chip optofluidic particle sorting based on phase gradient [208]. **e** Optofluidic particle sorting based on graphene nano-ribbons [209]

efficiency of about 80% for particles and the latter with a capture efficiency of up to 98% under the same conditions. In addition, optofluidic tweezers also play an extraordinary role in particle sorting. In 2018, Nan et al. demonstrated a multifunctional tunable optofluidic potential well for nanomanipulation by synchronizing optical phase gradient forces and fluid resistance, such as Fig. 12d [208]. They experimentally achieved controlled capture and transport of 150 nm gold nanoparticles in excess of 10 μm , and experimentally sorted 80 nm and 100 nm gold nanoparticles using an optical wire situation well with a tunable phase gradient. In addition, based on the simulation results, they further predicted that the optimization of the light field could enable the simultaneous sorting and capture of sub-50 nm gold nanoparticles with a sorting resolution of 1 nm. Subsequently, as in Fig. 12e shows that in 2023, Gholizadeh et al. proposed a novel graphene nano-ribbon-based optofluidic tweezers that can be used to manipulate and sort biological tissue particles with a radius of less than 2.5 nm [209]. The particles are transported to the main channel in the center of the structure through microfluidics, and then the graphene nanoribbons embedded in the silicon substrate are used to exert an optical force perpendicular to the direction of the main channel to the particles in the channel, so that the particle motion is offset and enters the subchannel. By adjusting the gap spacing between the graphene nanoribbon and the main channel, the particles of a specific size enter the corresponding sub-channel, and the sorting of particles of a specific size is realized. The combination of optofluidic and optical tweezers provides great efficiency, flexibility, and accuracy for nanomanipulation in microfluidics, which greatly broadens its application scenarios in the field of nanophotonics.

4.2.2 Biomedical applications

In addition to optical micromanipulation, optofluidic technology also has extraordinary performance in biomedical fields [210]. By greatly reducing the thermal effect, optofluidic can be used to capture and transport viruses that are difficult to manipulate with traditional optical manipulation techniques. As shown in Fig. 13a, in 2022, Shi et al. proposed a novel dielectric Si3N4 nanopore optical tweezer array system with stronger light field localization and greater optical well depth [211]. The optical force generated by this technology is sufficient to overcome the effects of drag in low-velocity fluids. Since the material does not absorb light, the photothermal effect is reduced, allowing it to retain the activity of bioparticles. Thus, versatile manipulation of low-flux unmodified viruses is achieved by adjusting the size and power of the laser. Not only can it capture, transport, and localize a single virus, but it can also isolate a specific size of virus from a large number of viruses in nanopores, thereby enabling virus purification. At the same time, the flow characteristics of microfluidics also help overcome the slow diffusion of samples in solution during biological testing, enabling fast and real-time analytical detection.

In 2017, Li et al. developed a nano-plasmonic biosensor for real-time monitoring of live secreted cytokines, such as Fig. 13b [212]. The nano-plasmon biosensor, consisting of an array of gold nanopores, supports extraordinary optical transmission (EOT), enabling high-throughput sensitive analysis of biomolecules. The nano-biosensor is integrated with an adjustable microfluidic unit module for the analysis of viable cells cultured under favorable culture conditions. Experimentally, they achieved a very high sensitivity for the direct detection of vascular endothelial growth factor (VEGF) in complex cell culture media. In addition, the application of optical fluidics technology can also be used to manipulate and sort cells. As an example, in 2024, Zhang et al. studied the mechanism of fiber optical tweezers manipulating cells through scattering force, using a single-mode fiber with a straight end to drive and sort cells, and derived the corresponding scattering force formula according to the T-matrix model. Based on this, they developed a single-mode optical tweezer system for cell sorting, and built an optical fluidic experimental platform that effectively integrates the optical system and a microfluidic chip, as shown in Fig. 13c [213]. The chip uses an extended cross-channel design to successfully achieve continuous sorting of yeast cells (8–10 μm diameter) and polystyrene microspheres (15–20 μm diameter) with a sorting efficiency of up to 86% and maintaining the viability of about 90% of yeast cells. Compared to other sorting systems, this system does not require labeling and enables continuous sorting with cell viability at a lower instrument cost.

5 Conclusion

Optical manipulation has revolutionized the control of microscopic and nanoscopic objects, with advancements in fiber-based techniques, metamaterials, and optofluidics expanding its capabilities and applications. These innovations have enabled breakthroughs in biological research, materials science, and nanotechnology. However, the field faces significant challenges. The complexity and bulkiness of conventional optical setups hinder integration and limit

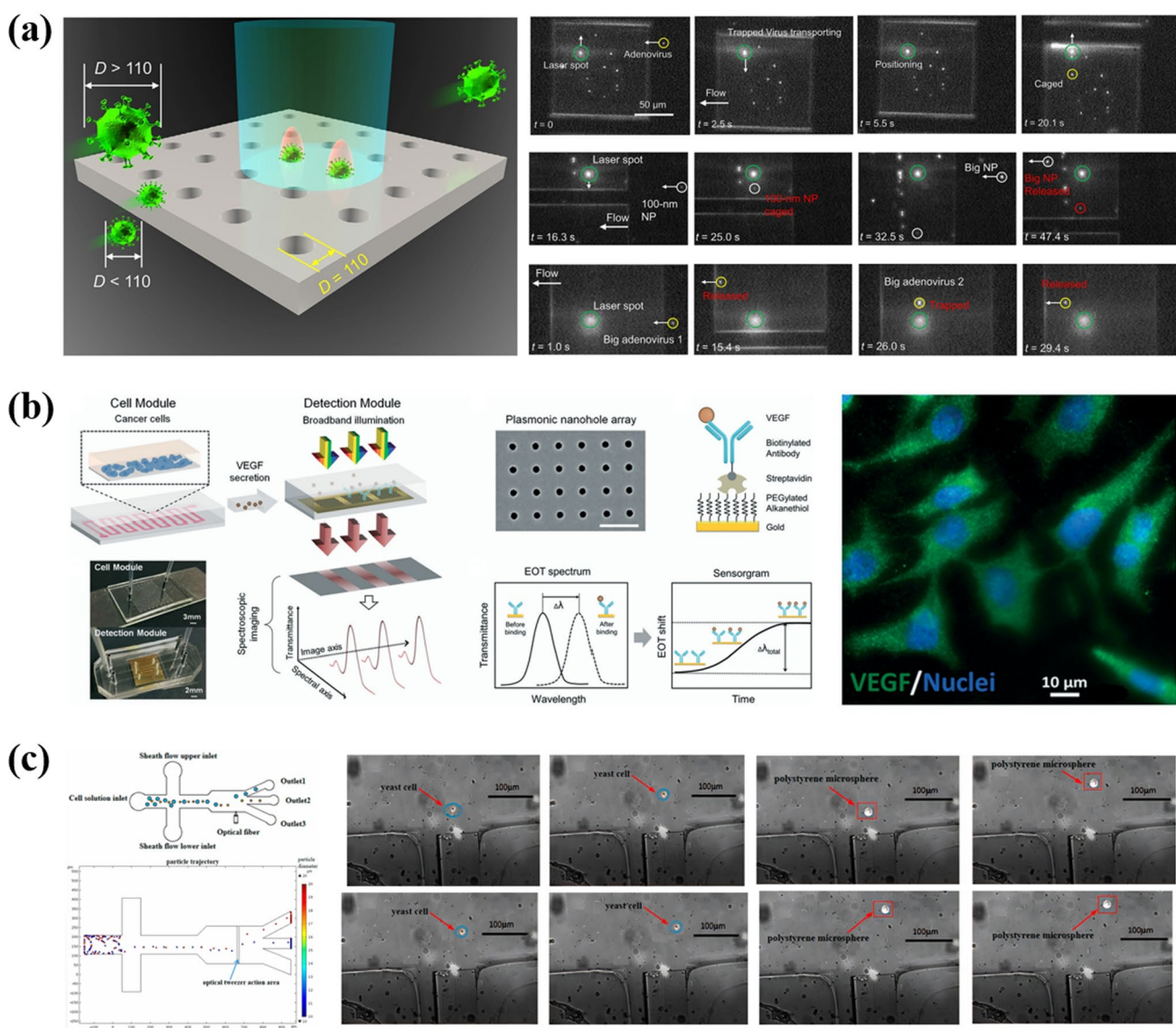


Fig. 13 Applications of optofluidic in Biomedicine. **a** Manipulation of viruses by using two-dimensional photonic crystal optical tweezers [211]. **b** Nano-plasmon biosensors based on optofluidic [212]. **c** Cell sorting based on integrated fiber optical tweezers and microfluidic chips [213]

use in certain environments. Overcoming these issues requires miniaturization and functional integration, such as fiber-based and on-chip optical manipulation systems. Additionally, enhancing trapping efficiency and resolution for smaller particles remains a key technical challenge. Emerging trends like machine learning for automated manipulation, quantum optical forces, and integration with nanophotonic technologies hold great promise. Machine learning can optimize light field distribution and enable real-time adjustments, while quantum optical forces may allow for more precise and sensitive manipulation. Integration with nanophotonic technologies could lead to more complex and efficient photonic systems. Looking ahead, the convergence of optical manipulation with these cutting-edge technologies will drive transformative innovations. Addressing specific technical challenges through focused research and development will further advance the field. This will require collaboration across disciplines and innovation in both theoretical and experimental approaches.

In summary, optical manipulation is poised to continue its transformative impact across various scientific and industrial domains, with future advancements promising even greater precision, efficiency, and versatility.

Acknowledgements We sincerely thank all the researchers who conduct the studies and contribute to harnessing optical forces with advanced nanophotonic structures. We also acknowledge the support of the National Program on Key Basic Research Project of China (2022YFA1404300), National Natural Science Foundation of China (No. 12325411, 62288101, 11774162), the Open Research Fund of the State Key Laboratory of Transient Optics and Photonics, Chinese Academy of Sciences (SKLST202218), the Fundamental Research Funds for the Central Universities (020414380175), the Natural Science Foundation of Jiangsu Province (No. BK20233001), and the Jiangsu Provincial Key Research and Development Program (BG2024029) for this work.

Author contributions T.L. initiated the idea, G.G and T.S. wrote the main manuscript text. All authors reviewed the manuscript.

Funding This work was supported by the National Program on Key Basic Research Project of China (2022YFA1404300), National Natural Science Foundation of China (No. 12325411, 62288101, 11774162), the Open Research Fund of the State Key Laboratory of Transient Optics and Photonics, Chinese Academy of Sciences (SKLST202218), the Fundamental Research Funds for the Central Universities (020414380175), the Natural Science Foundation of Jiangsu Province (No. BK20233001), and the Jiangsu Provincial Key Research and Development Program (BG2024029).

Data availability No datasets were generated or analysed during the current study.

Declarations

Ethics approval and Consent to participate Not applicable.

Consent to publish Not applicable.

Competing interest The authors declare no competing interests.

Open Access This article is licensed under a Creative Commons Attribution-NonCommercial-NoDerivatives 4.0 International License, which permits any non-commercial use, sharing, distribution and reproduction in any medium or format, as long as you give appropriate credit to the original author(s) and the source, provide a link to the Creative Commons licence, and indicate if you modified the licensed material. You do not have permission under this licence to share adapted material derived from this article or parts of it. The images or other third party material in this article are included in the article's Creative Commons licence, unless indicated otherwise in a credit line to the material. If material is not included in the article's Creative Commons licence and your intended use is not permitted by statutory regulation or exceeds the permitted use, you will need to obtain permission directly from the copyright holder. To view a copy of this licence, visit <http://creativecommons.org/licenses/by-nc-nd/4.0/>.

References

1. Ashkin A. Acceleration and trapping of particles by radiation pressure. *Phys Rev Lett.* 1970;24:156–9.
2. Ashkin A, Dziedzic JM, Bjorkholm JE, Chu S. Observation of a single-beam gradient force optical trap for dielectric particles. *Opt Lett.* 1986;11:288.
3. Smith SB, Cui Y, Bustamante C. Overstretching B-DNA: the elastic response of individual double-stranded and single-stranded DNA molecules. *Science.* 1996;271:795–9.
4. Svoboda K, Schmidt CF, Schnapp BJ, Block SM. Direct observation of kinesin stepping by optical trapping interferometry. *Nature.* 1993;365:721–7.
5. Finer JT, Simmons RM, Spudich JA. Single myosin molecule mechanics: piconewton forces and nanometre steps. *Nature.* 1994;368:113–9.
6. Schlosser F, Rehfeldt F, Schmidt CF. Force fluctuations in three-dimensional suspended fibroblasts. *Philos Trans R Soc Lond B Biol Sci.* 2015;370:20140028.
7. Grier DG. Optical tweezers in colloid and interface science. *Curr Opin Colloid Interface Sci.* 1997;2:264–70.
8. Marago OM, Jones PH, Gucciardi PG, Volpe G, Ferrari AC. Optical trapping and manipulation of nanostructures. *Nat Nanotechnol.* 2013;8:807–19.
9. Ashkin A. Optical trapping and manipulation of neutral particles using lasers. *Proc Natl Acad Sci USA.* 1997;94:4853–60.
10. Zhong MC, Wei XB, Zhou JH, Wang ZQ, Li YM. Trapping red blood cells in living animals using optical tweezers. *Nat Commun.* 2013;4:1768.
11. Liu Z, Guo C, Yang J, Yuan L. Tapered fiber optical tweezers for microscopic particle trapping: fabrication and application. *Opt Express.* 2006;14:12510–6.
12. Zhang H, Liu KK. Optical tweezers for single cells. *J R Soc Interface.* 2008;5:671–90.
13. Yuan Y, Lin Y, Gu B, Panwar N, Tjin SC, Song J, Qu J, Yong K-T. Optical trapping-assisted SERS platform for chemical and biosensing applications: design perspectives. *Coord Chem Rev.* 2017;339:138–52.
14. Ashkin A, Dziedzic JM. Optical trapping and manipulation of viruses and bacteria. *Science.* 1987;235:1517–20.
15. Yao J, Lai F, Fan Y, Wang Y, Huang SH, Leng B, Liang Y, Lin R, Chen S, Chen MK, Wu PC, Xiao S, Tsai DP. Nonlocal meta-lens with Huygens' bound states in the continuum. *Nat Commun.* 2024;15:6543.
16. Wang S, Wu PC, Su VC, Lai YC, Chen MK, Kuo HY, Chen BH, Chen YH, Huang TT, Wang JH, Lin RM, Kuan CH, Li T, Wang Z, Zhu S, Tsai DP. A broadband achromatic metalens in the visible. *Nat Nanotechnol.* 2018;13:227–32.
17. Lin RJ, Su VC, Wang S, Chen MK, Chung TL, Chen YH, Kuo HY, Chen JW, Chen J, Huang YT, Wang JH, Chu CH, Wu PC, Li T, Wang Z, Zhu S, Tsai DP. Achromatic metalens array for full-colour light-field imaging. *Nat Nanotechnol.* 2019;14:227–31.

18. Hua X, Wang Y, Wang S, Zou X, Zhou Y, Li L, Yan F, Cao X, Xiao S, Tsai DP, Han J, Wang Z, Zhu S. Ultra-compact snapshot spectral light-field imaging. *Nat Commun.* 2022;13:2732.
19. Wang S, Wu PC, Su VC, Lai YC, Hung Chu C, Chen JW, Lu SH, Chen J, Xu B, Kuan CH, Li T, Zhu S, Tsai DP. Broadband achromatic optical metasurface devices. *Nat Commun.* 2017;8:187.
20. Li T, Xu H, Panmai M, Shao T, Gao G, Xu F, Hu G, Wang S, Wang Z, Zhu S. Ultrafast metaphotonics. *Ultrafast Sci.* 2024;4:0074.
21. Li TY, Liu MJ, Hou JH, Yang X, Wang SB, Wang SM, Zhu SN, Tsai DP, Wang ZL. Chip-scale metaphotonic singularities: topological, dynamical, and practical aspects. *Chip.* 2024;3: 100109.
22. Li T, Liu M, Chen C, Li X, Hou J, Yang X, Wang S, Zhu S. Realization of spinful metaphotonic stokes skyrmions. *J Opt.* 2024;26:09LT01.
23. Li T, Chen Y, Fu B, Liu M, Wang J, Gao H, Wang S, Zhu S. Spin-selective trifunctional metasurfaces for deforming versatile nondiffractive beams along the optical trajectory. *Laser Photonics Rev.* 2024;18:2301372.
24. Xu X, Gao W, Li T, Shao T, Li X, Zhou Y, Gao G, Wang G, Yan S, Wang S, Yao B. Metasurfaces-empowered optical micromanipulation (Invited). *Acta Optica Sinica.* 2024;44:0500001.
25. Chen R, Bi Q, Li T, Wang S, Zhu S, Wang Z. Dual-wavelength chiral metasurfaces based on quasi-bound states in the continuum. *J Opt.* 2023;25: 045001.
26. Liu M, Li T, Ge Q, Wang S, Wang Z, Zhu S. Phase modulation mechanism and research progress of multifunctional metasurfaces. *Acta Opt Sinica.* 2022;42:2126004.
27. Chen R, Li T, Bi Q, Wang S, Zhu S, Wang Z. Quasi-bound states in the continuum-based switchable light-field manipulator. *Opt Mater Express.* 2022;12:1232.
28. Ren J, Li T, Fu B, Wang S, Wang Z, Zhu S. Wavelength-dependent multifunctional metalens devices via genetic optimization. *Opt Mater Express.* 2021;11:3908.
29. Li T, Li X, Yan S, Xu X, Wang S, Yao B, Wang Z, Zhu S. Generation and conversion dynamics of dual bessel beams with a photonic spin-dependent dielectric metasurface. *Phys Rev Appl.* 2021;15: 014059.
30. Li TY, Fu BY, Ren JZ, Wang SM, Wang ZL, Zhu SN. multidimensional light-field manipulation and applications based on optical metasurface. *Proc Spie.* 2021;11850:1185004.
31. Chen J, Ng J, Lin Z, Chan CT. Optical pulling force. *Nat Photonics.* 2011;5:531–4.
32. Novitsky A, Qiu CW, Wang H. Single gradientless light beam drags particles as tractor beams. *Phys Rev Lett.* 2011;107: 203601.
33. Zhang Y, Li T, Wang S, Wang Z, Zhu S. Polarization-dependent optical forces arising from fano interference. *Adv Phys Res.* 2023;2:2200048.
34. Juan ML, Righini M, Quidant R. Plasmon nano-optical tweezers. *Nat Photonics.* 2011;5:349–56.
35. Hoffman BD, Grashoff C, Schwartz MA. Dynamic molecular processes mediate cellular mechanotransduction. *Nature.* 2011;475:316–23.
36. Sleep J, Wilson D, Simmons R, Gratzer W. Elasticity of the red cell membrane and its relation to hemolytic disorders: an optical tweezers study. *Biophys J.* 1999;77:3085–95.
37. Wang H, Pumera M. Fabrication of Micro/Nanoscale Motors. *Chem Rev.* 2015;115:8704–35.
38. Williams BJ, Anand SV, Rajagopalan J, Saif MT. A self-propelled biohybrid swimmer at low Reynolds number. *Nat Commun.* 2014;5:3081.
39. Li J, Esteban-Fernandez de Avila B, Gao W, Zhang L, Wang J. Micro/nanorobots for biomedicine: delivery, surgery, sensing, and detoxification. *Sci Robot.* 2017;2:eaam6431.
40. Martel S. Microrobotics in the vascular network: present status and next challenges. *J Micro-Bio Robot.* 2013;8:41–52.
41. Gao W, Kagan D, Pak OS, Clawson C, Campuzano S, Chuluun-Erdene E, Shipton E, Fullerton EE, Zhang L, Lauga E, Wang J. Cargo-towing fuel-free magnetic nanoswimmers for targeted drug delivery. *Small.* 2012;8:460–7.
42. Psaltis D, Quake SR, Yang C. Developing optofluidic technology through the fusion of microfluidics and optics. *Nature.* 2006;442:381–6.
43. Wang MM, Tu E, Raymond DE, Yang JM, Zhang H, Hagen N, Dees B, Mercer EM, Forster AH, Kariv I, Marchand PJ, Butler WF. Microfluidic sorting of mammalian cells by optical force switching. *Nat Biotechnol.* 2005;23:83–7.
44. Guck J, Schinkinger S, Lincoln B, Wottawah F, Ebert S, Romeyke M, Lenz D, Erickson HM, Ananthakrishnan R, Mitchell D, Kas J, Ulwick S, Bilby C. Optical deformability as an inherent cell marker for testing malignant transformation and metastatic competence. *Biophys J.* 2005;88:3689–98.
45. Chiou PY, Ohta AT, Wu MC. Massively parallel manipulation of single cells and microparticles using optical images. *Nature.* 2005;436:370–2.
46. Nitta N, Sugimura T, Isozaki A, Mikami H, Hiraki K, Sakuma S, Iino T, Arai F, Endo T, Fujiwaki Y, Fukuzawa H, Hase M, Hayakawa T, Hiramatsu K, Hoshino Y, Inaba M, Ito T, Karakawa H, Kasai Y, Koizumi K, Lee S, Lei C, Li M, Maeno T, Matsusaka S, Murakami D, Nakagawa A, Oguchi Y, Oikawa M, Ota T, Shiba K, Shintaku H, Shirasaki Y, Suga K, Suzuki Y, Suzuki N, Tanaka Y, Tezuka H, Toyokawa C, Yalikun Y, Yamada M, Yamagishi M, Yamano T, Yasumoto A, Yatomi Y, Yazawa M, Di Carlo D, Hosokawa Y, Uemura S, Ozeki Y, Goda K. Intelligent image-activated cell sorting. *Cell.* 2018;175:266–76.
47. Vollmer F, Arnold S. Whispering-gallery-mode biosensing: label-free detection down to single molecules. *Nat Methods.* 2008;5:591–6.
48. Theberge AB, Courtois F, Schaefer Y, Fischlechner M, Abell C, Hollfelder F, Huck WT. Microdroplets in microfluidics: an evolving platform for discoveries in chemistry and biology. *Angew Chem Int Ed Engl.* 2010;49:5846–68.
49. Erickson D, Mandal S, Yang AH, Cordovez B. Nanobiosensors: optofluidic, electrical and mechanical approaches to biomolecular detection at the nanoscale. *Microfluid Nanofluidics.* 2008;4:33–52.
50. Roelkens G, Van Campenhout J, Brouckaert J, Van Thourhout D, Baets R, Romeo PR, Regreny P, Kazmierczak A, Seassal C, Letartre X, Hollinger G, Fedeli JM, Di Cioccio L, Laghae-Blanchard C. III-V/Si photonics by die-to-wafer bonding. *Mater Today.* 2007;10:36–43.
51. Crozier KB, Sundaramurthy A, Kino GS, Quate CF. Optical antennas: resonators for local field enhancement. *J Appl Phys.* 2003;94:4632–42.
52. Shi J, Ahmed D, Mao X, Lin SC, Lawit A, Huang TJ. Acoustic tweezers: patterning cells and microparticles using standing surface acoustic waves (SSAW). *Lab Chip.* 2009;9:2890–5.
53. Reiserer A, Rempe G. Cavity-based quantum networks with single atoms and optical photons. *Rev Mod Phys.* 2015;87:1379–418.
54. Monat C, Domachuk P, Eggleton BJ. Integrated optofluidics: a new river of light. *Nat Photonics.* 2007;1:106–14.
55. Constable A, Kim J, Mervis J, Zarinetchi F, Prentiss M. Demonstration of a fiber-optical light-force trap. *Opt Lett.* 1993;18:1867–9.
56. Lyons ER, Sonek GJ. Confinement and bistability in a tapered hemispherically lensed optical fiber trap. *Appl Phys Lett.* 1995;66:1584–6.
57. Kozo Taguchi KT, Masaru Tanaka MT, Masahiro Ikeda MI. Dual-beam trapping method for an object with large relative refractive index. *Jpn J Appl Phys.* 2000;39:1302.

58. Singer W, Frick M, Haller T, Dietl P, Stefan B, Monika R-M. Combined optical tweezers and optical stretcher in microscopy. In: Proceedings of SPIE, 2001; pp. 227–232.
59. Guck J, Ananthakrishnan R, Cunningham CC, Käs J. Stretching biological cells with light. *J Phys Condens Matter*. 2002;14:4843–56.
60. Rudd D, Lopez-Mariscal C, Summers M, Shahvisi A, Gutierrez-Vega JC, McGloin D. Fiber based optical trapping of aerosols. *Opt Express*. 2008;16:14550–60.
61. Singer W, Frick M, Bernet S, Ritsch-Marte M. Self-organized array of regularly spaced microbeads in a fiber-optical trap. *J Opt Soc Am B*. 2003;20:1568.
62. Jensen-McMullin C, Lee HP, Lyons ER. Demonstration of trapping, motion control, sensing and fluorescence detection of polystyrene beads in a multi-fiber optical trap. *Opt Express*. 2005;13:2634–42.
63. Wei MT, Yang KT, Karmenyan A, Chiou A. Three-dimensional optical force field on a Chinese hamster ovary cell in a fiber-optical dual-beam trap. *Opt Express*. 2006;14:3056–64.
64. Kreysing MK, Kiesling T, Fritsch A, Dietrich C, Guck JR, Kas JA. The optical cell rotator. *Opt Express*. 2008;16:16984–92.
65. Liu Y, Yu M. Investigation of inclined dual-fiber optical tweezers for 3D manipulation and force sensing. *Opt Express*. 2009;17:13624–38.
66. Xiao G, Yang K, Luo H, Chen X, Xiong W. Orbital rotation of trapped particle in a transversely misaligned dual-fiber optical trap. *IEEE Photonics J*. 2016;8:1–8.
67. Asadollahbaik A, Thiele S, Weber K, Kumar A, Drozella J, Sterl F, Herkommer AM, Giessen H, Fick J. Highly efficient dual-fiber optical trapping with 3D printed diffractive fresnel lenses. *ACS Photonics*. 2019;7:88–97.
68. Hongmei J, Yan L, Pengfei C, Qunfeng S, Qingqing M. Optical trapping force and sensing detection research based on optical fiber shapes and transmission modes. In: Proceedings of SPIE, 2014; p. 928310.
69. Taguchi K, Ueno H, Hiramatsu T, Ikeda M. Optical trapping of dielectric particle and biological cell using optical fibre. *Electron Lett*. 1997;33:413–4.
70. Xin H, Xu R, Li B. Optical trapping, driving, and arrangement of particles using a tapered fibre probe. *Sci Rep*. 2012;2:818.
71. Sang In E, Yasuhiro T, Takashi M, Terutake H. The 3D manipulation of a microsphere for nano-CMM probe using single fiber optical trapping. In: Proceedings of SPIE, 2006; p. 63261W.
72. Tong W, Xiaoyun T, Yaxun Z, Yu Z, Zhihai L. A novel single fiber optical tweezers based on GIMMF: simulation and experiment. In: Proceedings of SPIE, 2017; p. 103235A.
73. Liu Z, Liang P, Zhang Y, Lei J, Zhang Y, Yang J, Yuan L. A micro-particle launching apparatus based on mode-division-multiplexing technology. *Opt Commun*. 2015;342:30–5.
74. Liu Z, Liang P, Zhang Y, Zhang Y, Zhao E, Yang J, Yuan L. Micro particle launcher/cleaner based on optical trapping technology. *Opt Express*. 2015;23:8650–8.
75. Chen W-Y, Hung T-Y, Hsieh Y-K, Po-Hung Li L, Chen Y-B, Minin OV, Minin IV, Liu C-Y. Numerical and experimental demonstrations of optical trapping and manipulation of a selective red blood cell using a photonic hook based on broken symmetry tapered fiber probe. *Opt Laser Technol*. 2025;180: 111520.
76. Xu L, Li Y, Li B. Size-dependent trapping and delivery of submicro-spheres using a submicrofibre. *New J Phys*. 2012;14: 033020.
77. Li Y, Xu L, Li B. Optical delivery of nanospheres using arbitrary bending nanofibers. *J Nanopart Res*. 2012;14:799.
78. Daly M, Truong VG, Chormaic SN. Evanescent field trapping of nanoparticles using nanostructured ultrathin optical fibers. *Opt Express*. 2016;24:14470–82.
79. Hong LI, Ying-xin ZHU, Ya-ni Z, Hai-bo W, Ming-li D, Lian-qing ZHU. Advances in optical fiber tweezer technology based on hetero-core fiber. *Chin Opt*. 2023;16:1293–304.
80. Taylor R, Hnatovsky C. Particle trapping in 3-D using a single fiber probe with an annular light distribution. *Opt Express*. 2003;11:2775–82.
81. Yuan L, Liu Z, Yang J, Guan C. Twin-core fiber optical tweezers. *Opt Express*. 2008;16:4559–66.
82. Zhang Y, Liang P, Lei J, Wang L, Liu Z, Yang J, Yuan L. Multi-dimensional manipulation of yeast cells using a LP₁₁ mode beam. *J Lightwave Technol*. 2014;32:1098–103.
83. Zhang Y, Zhao L, Chen Y, Liu Z, Zhang Y, Zhao E, Yang J, Yuan L. Single optical tweezers based on elliptical core fiber. *Opt Commun*. 2016;365:103–7.
84. Velazquez-Benitez AM, Guerra-Santillan KY, Caudillo-Viurquez R, Antonio-Lopez JE, Amezcu-Correa R, Hernandez-Cordero J. Optical trapping and micromanipulation with a photonic lantern-mode multiplexer. *Opt Lett*. 2018;43:1303–6.
85. Anastasiadi G, Leonard M, Paterson L, Macpherson WN. Fabrication and characterization of machined multi-core fiber tweezers for single cell manipulation. *Opt Express*. 2018;26:3557–67.
86. Liu J, Guan C, Chen H, Liu B, Cheng T, Yang J, Shi J, Yuan L. Dual-core optical fiber tweezers based on all-dielectric metasurface. *Opt Commun*. 2023;531: 129232.
87. Zhu Y, Li H, Wang Y, Cui X, Zhu L. Focusing property and optical field modulation of three-core fiber optical tweezers. *J Quant Spectrosc Radiat Transf*. 2024;314: 108865.
88. Rong Q, Zhou Y, Yin X, Shao Z, Qiao X. Higher-order micro-fiber modes for Escherichia coli manipulation using a tapered seven-core fiber. *Biomed Opt Express*. 2017;8:4096–107.
89. Zhang X, Yuan T, Yang S, Yang J, Yuan L. Optical trajectory transport device based on a three-core fiber. *Opt Laser Technol*. 2021;140: 107076.
90. Li T, Xu X, Fu B, Wang S, Li B, Wang Z, Zhu S. Integrating the optical tweezers and spanner onto an individual single-layer metasurface. *Photonics Res*. 2021;9:1062–8.
91. Nan F, Yan Z. Synergy of intensity, phase, and polarization enables versatile optical nanomanipulation. *Nano Lett*. 2020;20:2778–83.
92. Nan F, Rodriguez-Fortuno FJ, Yan S, Kingsley-Smith JJ, Ng J, Yao B, Yan Z, Xu X. Creating tunable lateral optical forces through multipolar interplay in single nanowires. *Nat Commun*. 2023;14:6361.
93. Min C, Shen Z, Shen J, Zhang Y, Fang H, Yuan G, Du L, Zhu S, Lei T, Yuan X. Focused plasmonic trapping of metallic particles. *Nat Commun*. 2013;4:2891.
94. Samadi M, Vasini S, Darbari S, Khorshad AA, Reihani SNS, Moravvej-Farshi MK. Hexagonal arrays of gold triangles as plasmonic tweezers. *Opt Express*. 2019;27:14754–66.

95. Kotsifaki DG, Truong VG, Nic Chormaic S. Dynamic multiple nanoparticle trapping using metamaterial plasmonic tweezers. *Appl Phys Lett.* 2021;118:021107.
96. Liu W, Min C, Zhang Y. Selective plasmonic trapping of nano-particles by Archimedes metalens. *Opt Express.* 2023;31:35354–62.
97. Zaman MA, Hesselink L. Dynamically controllable plasmonic tweezers using C-shaped nano-engravings. *Appl Phys Lett.* 2022;121:181108.
98. Bouloumis TD, Kotsifaki DG, Nic Chormaic S. Enabling self-induced back-action trapping of gold nanoparticles in metamaterial plasmonic tweezers. *Nano Lett.* 2023;23:4723–31.
99. Wang Y, Wei S, Ju Z, Min C, Somekh M, Yuan X. Dynamic optical tweezers for metallic particle manipulation via tunable plasmonic fields. *Photonics Res.* 2024;12:1840–5.
100. Zheng S, Yu Y, Zhou X, Fu B, Wang S, Wang Z, Zhu S. Research on multidimensional optical imaging empowered by metasurfaces (Invited). *Laser Optoelectron Prog.* 2024;61:1611001.
101. Fu B, Bi Q, Zheng S, Peng Y, Wang S, Cao X, Wang Z, Zhu S. Advanced metasurface imaging and display based on multidimensional light field manipulation (Invited). *Acta Optica Sinica.* 2024;44:1400001.
102. Sun Z, Li T, Kuang S, Yun X, He M, Fu B, Fu Y, Zhao T, Wang S, Liang Y, Wang S, Lei M. On-demand quick metasurface design with neighborhood attention transformer. *arXiv:2412.08405* (2025) <https://arxiv.org/abs/2412.08405>.
103. Fu B, Zhou X, Li T, Zhu H, Liu Z, Zheng S, Zhou Y, Yu Y, Cao X, Wang S, Wang Z, Zhu S. Miniaturized high-efficiency snapshot polarimetric stereoscopic imaging. *Optica.* 2025;12:391–8.
104. Markovich H, Shishkin IL, Hendler N, Ginzburg P. Optical manipulation along an optical axis with a polarization sensitive meta-lens. *Nano Lett.* 2018;18:5024–9.
105. Chantakit T, Schlickriede C, Sain B, Meyer F, Weiss T, Chattham N, Zentgraf T. All-dielectric silicon metalens for two-dimensional particle manipulation in optical tweezers. *Photonics Res.* 2020;8:1435–40.
106. Wang Y, Peng M, Cheng W, Peng Z, Cheng H, Ren X, Zang S, Shuai Y, Liu H, Wu J, Yang J. Manipulation force analysis of nanoparticles with ultra-high numerical aperture metalens. *Opt Express.* 2022;30:28479–91.
107. Yu G, Guo J, Shi J, Mao X, Ding H, Zheng H, Shen C. On-chip multi-trap optical tweezers based on a guided wave-driven metalens. *Opt Lett.* 2024;49:1225–8.
108. Yang D, Zhang J, Zhang P, Liang H, Ma J, Li J, Wang X-H. Optical trapping and manipulating with a transmissive and polarization-insensitive metalens. *Nanophotonics.* 2024;13:2781–9.
109. Shi Y, Zhu T, Liu AQ, Zhou LM, Nieto-Vesperinas M, Hassanfiroozi A, Liu J, Tsai DP, Li Z, Ding W, Wang F, Li H, Song Q, Xu X, Li B, Cheng X, Wu PC, Chan CT, Qiu CW. Inverse optical torques on dielectric nanoparticles in elliptically polarized light waves. *Phys Rev Lett.* 2022;129: 053902.
110. Xu X, Nieto-Vesperinas M, Zhou Y, Zhang Y, Li M, Rodriguez-Fortuno FJ, Yan S, Yao B. Gradient and curl optical torques. *Nat Commun.* 2024;15:6230.
111. Zhou Y, Zhang Y, Xu X, Nieto-Vesperinas M, Yan S, Li M, Gao W, Zhang Y, Yao B. Optical forces on multipoles induced by the belinfante spin momentum. *Laser Photonics Rev.* 2023;17:2300245.
112. Hu Y, Kingsley-Smith JJ, Nikkhoud M, Sabin JA, Rodriguez-Fortuno FJ, Xu X, Millen J. Structured transverse orbital angular momentum probed by a levitated optomechanical sensor. *Nat Commun.* 2023;14:2638.
113. Liu C, Huang Z, Huang S, Zhang Y, Li B, Nan F, Zheng Y. Robotic nanomanipulation based on spatiotemporal modulation of optical gradients. *ACS Nano.* 2024;18:19391–400.
114. Gao WY, Zhou Y, Li X, Zhang YN, Zhang Q, Li MM, Yu XH, Yan SH, Xu XH, Yao BL. Particle delivery in generalized optical vortex conveyor belts with a uniform orbital flow. *Photonics Res.* 2024;12:2881–90.
115. Liu X, Li Y, Xu X, Zhang Y, Li B. Optical fan for single-cell screening. *J Biophotonics.* 2019;13: e201900155.
116. Neuman KC, Block SM. Optical trapping. *Rev Sci Instrum.* 2004;75:2787–809.
117. Block SM, Goldstein LS, Schnapp BJ. Bead movement by single kinesin molecules studied with optical tweezers. *Nature.* 1990;348:348–52.
118. Thoumine O, Ott A. Time scale dependent viscoelastic and contractile regimes in fibroblasts probed by microplate manipulation. *J Cell Sci.* 1997;110(Pt 17):2109–16.
119. Henon S, Lenormand G, Richert A, Gallet F. A new determination of the shear modulus of the human erythrocyte membrane using optical tweezers. *Biophys J.* 1999;76:1145–51.
120. Liu X, Li Y, Xu X, Zhang Y, Li B. Red-blood-cell-based microlens: application to single-cell membrane imaging and stretching. *ACS Appl Bio Mater.* 2019;2:2889–95.
121. Berns MW, Aist J, Edwards J, Strahs K, Girton J, McNeill P, Rattner JB, Kitzes M, Hammer-Wilson M, Liaw LH, Siemens A, Koonce M, Peterson S, Brenner S, Burt J, Walter R, Bryant PJ, van Dyk D, Coulombe J, Cahill T, Berns GS. Laser microsurgery in cell and developmental biology. *Science.* 1981;213:505–13.
122. Gao Q, Wang W, Li X, Li Y, Ferraro P, Jiao X, Liu X, Zhang Y, Li B. Cell nucleus as endogenous biological micropump. *Biosens Bioelectron.* 2021;182: 113166.
123. Liu X, Gao Q, Wu S, Qin H, Zhang T, Zheng X, Li B. Optically manipulated neutrophils as native microcrafts in vivo. *ACS Cent Sci.* 2022;8:1017–27.
124. Liu X, Huang J, Li Y, Zhang Y, Li B. Rotation and deformation of human red blood cells with light from tapered fiber probes. *Nanophotonics.* 2017;6:309–16.
125. Li Y, Liu X, Xu X, Xin H, Zhang Y, Li B. Red-blood-cell waveguide as a living biosensor and micromotor. *Adv Func Mater.* 2019;29:1905568.
126. Suresh S. Biomechanics and biophysics of cancer cells☆. *Acta Mater.* 2007;55:3989–4014.
127. Sraj I, Eggleton CD, Jimenez R, Hoover E, Squier J, Chichester J, Marr DW. Cell deformation cytometry using diode-bar optical stretchers. *J Biomed Opt.* 2010;15: 047010.
128. Fraczkowska K, Bacia M, Przybylo M, Drabik D, Kaczorowska A, Rybka J, Stefanko E, Drobczynski S, Masajada J, Podbielska H, Wrobel T, Kopaczynska M. Alterations of biomechanics in cancer and normal cells induced by doxorubicin. *Biomed Pharmacother.* 2018;97:1195–203.

129. Schmidt CE, Horwitz AF, Lauffenburger DA, Sheetz MP. Integrin-cytoskeletal interactions in migrating fibroblasts are dynamic, asymmetric, and regulated. *J Cell Biol.* 1993;123:977–91.
130. Hashimoto S, Yoshida A, Ohta T, Taniguchi H, Sadakane K, Yoshikawa K. Formation of stable cell-cell contact without a solid/gel scaffold: non-invasive manipulation by laser under depletion interaction with a polymer. *Chem Phys Lett.* 2016;655–656:11–6.
131. Diao Z, Jing X, Hou X, Meng Y, Zhang J, Wang Y, Ji Y, Ge A, Wang X, Liang Y, Xu J, Ma B. Artificial intelligence-assisted automatic raman-activated cell sorting (AI-RACS) system for mining specific functional microorganisms in the microbiome. *Anal Chem.* 2024;96:18416–26.
132. Chan JW. Recent advances in laser tweezers Raman spectroscopy (LTRS) for label-free analysis of single cells. *J Biophotonics.* 2013;6:36–48.
133. Ashkin A. History of optical trapping and manipulation of small-neutral particle, atoms, and molecules. *IEEE J Sel Top Quantum Electron.* 2000;6:841–56.
134. Sasaki K, Koshioka M, Misawa H, Kitamura N, Masuhara H. Pattern formation and flow control of fine particles by laser-scanning micro-manipulation. *Opt Lett.* 1991;16:1463–5.
135. Dufresne ER, Grier DG. Optical tweezer arrays and optical substrates created with diffractive optics. *Rev Sci Instrum.* 1998;69:1974–7.
136. Curtis JE, Koss BA, Grier DG. Dynamic holographic optical tweezers. *Optics Communications.* 2002;207:169–75.
137. Akselrod GM, Timp W, Mirsaidov U, Zhao Q, Li C, Timp R, Timp K, Matsudaira P, Timp G. Laser-guided assembly of heterotypic three-dimensional living cell microarrays. *Biophys J.* 2006;91:3465–73.
138. Kirkham GR, Britchford E, Upton T, Ware J, Gibson GM, Devaud Y, Ehrbar M, Padgett M, Allen S, Buttery LD, Shakesheff K. Precision assembly of complex cellular microenvironments using holographic optical tweezers. *Sci Rep.* 2015;5:8577.
139. Bambardekar K, Clement R, Blanc O, Chardes C, Lenne PF. Direct laser manipulation reveals the mechanics of cell contacts in vivo. *Proc Natl Acad Sci U S A.* 2015;112:1416–21.
140. Muhammed I, Chowdhury F, Maruthamuthu V. Biophysical tools to study cellular mechanotransduction. *Bioeng (Basel).* 2017;4:3390.
141. Agarwal P, Zhao S, Bielecki P, Rao W, Choi JK, Zhao Y, Yu J, Zhang W, He X. One-step microfluidic generation of pre-hatching embryo-like core-shell microcapsules for miniaturized 3D culture of pluripotent stem cells. *Lab Chip.* 2013;13:4525–33.
142. Yousafzai MS, Ndoye F, Coceano G, Niemela J, Bonin S, Scoles G, Cojoc D. Substrate-dependent cell elasticity measured by optical tweezers indentation. *Opt Lasers Eng.* 2016;76:27–33.
143. Tan Y, Sun D, Wang J, Huang W. Mechanical characterization of human red blood cells under different osmotic conditions by robotic manipulation with optical tweezers. *IEEE Trans Biomed Eng.* 2010;57:1816–25.
144. Cordero ML, Verneuil E, Gallaire F, Baroud CN. Time-resolved temperature rise in a thin liquid film due to laser absorption. *Phys Rev E Stat Nonlin Soft Matter Phys.* 2009;79: 011201.
145. Bunea AI, Glückstad J. Strategies for optical trapping in biological samples: aiming at microrobotic surgeons. *Laser Photonics Rev.* 2019;13:1800227.
146. Memmolo P, Miccio L, Paturzo M, Caprio GD, Coppola G, Netti PA, Ferraro P. Recent advances in holographic 3D particle tracking. *Adv Opt Photonics.* 2015;7:713–55.
147. Grier DG. A revolution in optical manipulation. *Nature.* 2003;424:810–6.
148. Nieto-Vesperinas M, Xu X. The complex Maxwell stress tensor theorem: the imaginary stress tensor and the reactive strength of orbital momentum. A novel scenery underlying electromagnetic optical forces. *Light Sci Appl.* 2022;11:297.
149. Zhou Y, Xu X, Zhang Y, Li M, Yan S, Nieto-Vesperinas M, Li B, Qiu CW, Yao B. Observation of high-order imaginary Poynting momentum optomechanics in structured light. *Proc Natl Acad Sci USA.* 2022;119: e2209721119.
150. Nan F, Li X, Zhang S, Ng J, Yan Z. Creating stable trapping force and switchable optical torque with tunable phase of light. *Sci Adv.* 2022;8:eadd6664.
151. Shi Y, Song Q, Toftul I, Zhu T, Yu Y, Zhu W, Tsai DP, Kivshar Y, Liu AQ. Optical manipulation with metamaterial structures. *Appl Phys Rev.* 2022;9: 031303.
152. Liu M, Zentgraf T, Liu Y, Bartal G, Zhang X. Light-driven nanoscale plasmonic motors. *Nat Nanotechnol.* 2010;5:570–3.
153. Hong X, Xu B, Li G, Nan F, Wang X, Liang Q, Dong W, Dong W, Sun H, Zhang Y, Li C, Fu R, Wang Z, Shen G, Wang Y, Yao Y, Zhang S, Li J. Optoelectronically navigated nano-kirigami microrotors. *Sci Adv.* 2024;10:eadn7582.
154. Tanaka YY, Albelia P, Rahmani M, Giannini V, Maier SA, Shimura T. Plasmonic linear nanomotor using lateral optical forces. *Sci Adv.* 2020;6:eabc3726.
155. Wu X, Ehehalt R, Razinskas G, Feichtner T, Qin J, Hecht B. Light-driven microdrones. *Nat Nanotechnol.* 2022;17:477–84.
156. Ilic O, Kaminer I, Zhen B, Miller OD, Buljan H, Soljacic M. Topologically enabled optical nanomotors. *Sci Adv.* 2017;3: e1602738.
157. Liang Z, Teal D, Fan DE. Light programmable micro/nanomotors with optically tunable in-phase electric polarization. *Nat Commun.* 2019;10:5275.
158. Tanaka YY, Shimura T. Tridirectional polarization routing of light by a single triangular plasmonic nanoparticle. *Nano Lett.* 2017;17:3165–70.
159. Andren D, Baranov DG, Jones S, Volpe G, Verre R, Kall M. Microscopic metavehicles powered and steered by embedded optical metasurfaces. *Nat Nanotechnol.* 2021;16:970–4.
160. Qin H, Redjem W, Kante B. Tunable and enhanced optical force with bound state in the continuum. *Opt Lett.* 2022;47:1774–7.
161. Li T, Kingsley-Smith JJ, Hu Y, Xu X, Yan S, Wang S, Yao B, Wang Z, Zhu S. Reversible lateral optical force on phase-gradient metasurfaces for full control of metavehicles. *Opt Lett.* 2023;48:255–8.
162. Engay E, Shanei M, Mylnikov V, Wang G, Johansson P, Volpe G, Käll M. Transverse optical gradient force in untethered rotating metaspiners. *Light Sci Appl.* 2025;14:38.
163. Ilic O, Atwater HA. Self-stabilizing photonic levitation and propulsion of nanostructured macroscopic objects. *Nat Photonics.* 2019;13:289–95.
164. Li T, Liu M, Qin J, Hou J, Ren J, Liu Y, Yang X, Chu H, Lai Y, Wang S, Jiang J-H, Chan CT, Zhu S. Configurable topological photonic polycrystal based on synthetic hybrid dimension. *Natl Sci Rev.* 2025. <https://doi.org/10.1093/nsr/nwaf107>.
165. Wiederhecker GS, Chen L, Gondarenko A, Lipson M. Controlling photonic structures using optical forces. *Nature.* 2009;462:633–6.
166. Apiratikul P, Wathen JJ, Porkolab GA, Wang B, He L, Murphy TE, Richardson CJ. Enhanced continuous-wave four-wave mixing efficiency in nonlinear AlGaAs waveguides. *Opt Express.* 2014;22:26814–24.
167. Li M, Pernice WHP, Tang HX. Tunable bipolar optical interactions between guided lightwaves. *Nat Photonics.* 2009;3:464–8.

168. Wiederhecker GS, Manipatruni S, Lee S, Lipson M. Broadband tuning of optomechanical cavities. *Opt Express*. 2011;19:2782–90.
169. Gong Y, Makarova M, Yerci S, Li R, Stevens MJ, Baek B, Nam SW, Hadfield RH, Dorenbos SN, Zwillaer V, Vuckovic J, Dal Negro L. Linewidth narrowing and Purcell enhancement in photonic crystal cavities on an Er-doped silicon nitride platform. *Opt Express*. 2010;18:2601–12.
170. Zhang M, Wiederhecker GS, Manipatruni S, Barnard A, McEuen P, Lipson M. Synchronization of micromechanical oscillators using light. *Phys Rev Lett*. 2012;109: 233906.
171. Phare CT, Daniel Lee Y-H, Cardenas J, Lipson M. Graphene electro-optic modulator with 30 GHz bandwidth. *Nat Photonics*. 2015;9:511–4.
172. Otterstrom NT, Behunin RO, Kittlaus EA, Wang Z, Rakich PT. A silicon Brillouin laser. *Science*. 2018;360:1113–6.
173. Bogaerts W, Perez D, Capmany J, Miller DAB, Poon J, Englund D, Morichetti F, Melloni A. Programmable photonic circuits. *Nature*. 2020;586:207–16.
174. Mourigas-Alexandris G, Tsakyridis A, Passalis N, Tefas A, Vrysokinos K, Pleros N. An all-optical neuron with sigmoid activation function. *Opt Express*. 2019;27:9620–30.
175. Bauters JF, Heck MJR, Dai D, Barton JS, Blumenthal DJ, Bowers JE. Ultralow-loss planar Si3N4 waveguide polarizers. *IEEE Photonics J*. 2013;5:6600207–6600207.
176. Benedikovic D, Alonso-Ramos C, Cheben P, Schmid JH, Wang S, Xu DX, Lapointe J, Janz S, Halir R, Ortega-Monux A, Wanguemert-Perez JG, Molina-Fernandez I, Fedeli JM, Vivien L, Dado M. High-directionality fiber-chip grating coupler with interleaved trenches and sub-wavelength index-matching structure. *Opt Lett*. 2015;40:4190–3.
177. Lin S, Crozier KB. Planar silicon microrings as wavelength-multiplexed optical traps for storing and sensing particles. *Lab Chip*. 2011;11:4047–51.
178. Yulaev A, Zhu W, Zhang C, Westly DA, Lezec HJ, Agrawal A, Aksyuk V. Metasurface-integrated photonic platform for versatile free-space beam projection with polarization control. *ACS Photonics*. 2019;6:2902–9.
179. Marchetti R, Lacava C, Carroll L, Grankowski K, Minzioni P. Coupling strategies for silicon photonics integrated chips [Invited]. *Photonics Res*. 2019;7:201–39.
180. Safavi-Naeini AH, Mayer Alegre TP, Chan J, Eichenfield M, Winger M, Lin Q, Hill JT, Chang DE, Painter O. Electromagnetically induced transparency and slow light with optomechanics. *Nature*. 2011;472:69–73.
181. Wang J, Sciarri F, Laing A, Thompson MG. Integrated photonic quantum technologies. *Nat Photonics*. 2019;14:273–84.
182. Povinelli ML, Loncar M, Ibanescu M, Smythe EJ, Johnson SG, Capasso F, Joannopoulos JD. Evanescent-wave bonding between optical waveguides. *Opt Lett*. 2005;30:3042–4.
183. Vlasov Y, McNab S. Losses in single-mode silicon-on-insulator strip waveguides and bends. *Opt Express*. 2004;12:1622–31.
184. Vlasov YA, O’Boyle M, Hamann HF, McNab SJ. Active control of slow light on a chip with photonic crystal waveguides. *Nature*. 2005;438:65–9.
185. Selvaraja SK, Bogaerts W, Dumon P, Van Thourhout D, Baets R. Subnanometer linewidth uniformity in silicon nanophotonic waveguide devices using CMOS fabrication technology. *IEEE J Sel Top Quantum Electron*. 2010;16:316–24.
186. Dionne JA, Sweatlock LA, Atwater HA, Polman A. Plasmon slot waveguides: towards chip-scale propagation with subwavelength-scale localization. *Phys Rev B*. 2006;73: 035407.
187. Taillaert D, Bogaerts W, Bienstman P, Krauss TF, Van Daele P, Moerman I, Verstuyft S, De Mesel K, Baets R. An out-of-plane grating coupler for efficient butt-coupling between compact planar waveguides and single-mode fibers. *IEEE J Quantum Electron*. 2002;38:949–55.
188. Li Q, Davanço M, Srinivasan K. Efficient and low-noise single-photon-level frequency conversion interfaces using silicon nanophotonics. *Nat Photonics*. 2016;10:406–14.
189. Romagnoli M, Sorianello V, Midrio M, Koppens FHL, Huyghebaert C, Neumaier D, Galli P, Templ W, D’Errico A, Ferrari AC. Graphene-based integrated photonics for next-generation datacom and telecom. *Nat Rev Mater*. 2018;3:392–414.
190. Haffner C, Chelladurai D, Fedoryshyn Y, Josten A, Baeuerle B, Heni W, Watanabe T, Cui T, Cheng B, Saha S, Elder DL, Dalton LR, Boltasseva A, Shalaev VM, Kinsey N, Leuthold J. Low-loss plasmon-assisted electro-optic modulator. *Nature*. 2018;556:483–6.
191. Dory C, Vercruyse D, Yang KY, Sapra NV, Rugar AE, Sun S, Lukin DM, Piggott AY, Zhang JL, Radulaski M, Lagoudakis KG, Su L, Vuckovic J. Inverse-designed diamond photonics. *Nat Commun*. 2019;10:3309.
192. Cheng Q, Bahadori M, Glick M, Rumley S, Bergman K. Recent advances in optical technologies for data centers: a review. *Optica*. 2018;5:1354–70.
193. Yang AH, Moore SD, Schmidt BS, Klug M, Lipson M, Erickson D. Optical manipulation of nanoparticles and biomolecules in sub-wavelength slot waveguides. *Nature*. 2009;457:71–5.
194. Cai H, Poon AW. Optical manipulation and transport of microparticles on silicon nitride microring-resonator-based add-drop devices. *Opt Lett*. 2010;35:2855–7.
195. Xu Q, Lipson M. All-optical logic based on silicon micro-ring resonators. *Opt Express*. 2007;15:924–9.
196. Rudolph T. Why I am optimistic about the silicon-photonic route to quantum computing. *APL Photonics*. 2017;2:030901.
197. Feldmann J, Youngblood N, Karpov M, Gehring H, Li X, Stappers M, Le Gallo M, Fu X, Lukashchuk A, Raja AS, Liu J, Wright CD, Sebastian A, Kippinen TJ, Pernice WHP, Bhaskaran H. Publisher correction: parallel convolutional processing using an integrated photonic tensor core. *Nature*. 2021;591:E13.
198. Zhu Y, You M, Shi Y, Huang H, Wei Z, He T, Xiong S, Wang Z, Cheng X. Optofluidic tweezers: efficient and versatile micro/nano-manipulation tools. *Micromachines*. 2023;14:1326.
199. Yang S, Hong C, Zhu G, Anyika T, Hong I, Ndukaife JC. Recent advancements in nanophotonics for optofluidics. *Adv Phys X*. 2024;9:1–47.
200. Liu X, Gao Q, Zhang Y, Li Y, Li B. In vivo optofluidic switch for controlling blood microflow. *Adv Sci*. 2020;7:2001414.
201. Liu X, Wu Y, Xu X, Li Y, Zhang Y, Li B. Bidirectional transport of nanoparticles and cells with a bio-conveyor belt. *Small*. 2019;15:1905209.
202. Liu X, Huang J, Li Y, Zhang Y, Li B. Optofluidic organization and transport of cell chain. *J Biophotonics*. 2017;10:1627–35.
203. Nan F, Yan Z. Optical sorting at the single-particle level with single-nanometer precision using coordinated intensity and phase gradient forces. *ACS Nano*. 2020;14:7602–9.
204. Gao Y, Harder R, Southworth SH, Guest JR, Huang X, Yan Z, Ocola LE, Yifat Y, Sule N, Ho PJ, Pelton M, Scherer NF, Young L. Three-dimensional optical trapping and orientation of microparticles for coherent X-ray diffraction imaging. *Proc Natl Acad Sci U S A*. 2019;116:4018–24.

205. Li X, Yang Y, Yan S, Gao W, Zhou Y, Yu X, Bai C, Dan D, Xu X, Yao B. Artificial potential field-empowered dynamic holographic optical tweezers for particle-array assembly and transformation. *Photonix*. 2024;5:32.
206. Lasnoy E, Wagner O, Edri E, Shpaisman H. Drag controlled formation of polymeric colloids with optical traps. *Lab Chip*. 2019;19:3543–51.
207. Walker ZJ, Wells T, Belliston E, Walker SB, Zeller C, Sampad MJN, Saiduzzaman SM, Schmidt H, Hawkins AR. Optofluidic particle manipulation: optical trapping in a thin-membrane microchannel. *Biosensors*. 2022;12:690.
208. Nan F, Yan Z. Creating multifunctional optofluidic potential wells for nanoparticle manipulation. *Nano Lett*. 2018;18:7400–6.
209. Gholizadeh E, Jafari B, Golmohammadi S. Graphene-based optofluidic tweezers for refractive-index and size-based nanoparticle sorting, manipulation, and detection. *Sci Rep*. 2023;13:1975.
210. Zhang T, Wu S, Qin H, Wu H, Liu X, Li B, Zheng X. An optically controlled virtual microsensor for biomarker detection *in vivo*. *Adv Mater*. 2022;34:2205760.
211. Shi Y, Wu Y, Chin LK, Li Z, Liu J, Chen MK, Wang S, Zhang Y, Liu PY, Zhou X, Cai H, Jin W, Yu Y, Yu R, Huang W, Yap PH, Xiao L, Ser W, Nguyen TT B, Lin YT, Wu PC, Liao J, Wang F, Chan CT, Kivshar Y, Tsai DP, Liu AQ. Multifunctional virus manipulation with large-scale arrays of all-dielectric resonant nanocavities. *Laser Photonics Rev*. 2022;16:2100197.
212. Li X, Soler M, Özdemir CI, Belushkin A, Yesilköy F, Altug H. Plasmonic nanohole array biosensor for label-free and real-time analysis of live cell secretion. *Lab Chip*. 2017;17:2208–17.
213. Zhang Y, Zhang T, Zhang X, Cheng J, Zhang S. Label-free continuous cell sorting using optofluidic chip. *Micromachines*. 2024;15:818.

Publisher's Note Springer Nature remains neutral with regard to jurisdictional claims in published maps and institutional affiliations.